Tetracene Dimers: A Platform for Intramolecular Down- and Up-conversion

Yifan Bo,[†,a] Yuxuan Hou,[†,b] Dominik Thiel,[†,a] René Weiß,[a] Timothy Clark,[c] Michael J. Ferguson,[b] Rik R. Tykwinski,[*,b] Dirk M. Guldi[*,a]

a Department of Chemistry and Pharmacy & Interdisciplinary Center for Molecular Materials (ICMM), Friedrich-Alexander-Universität Erlangen-Nürnberg, Egerlandstr. 3, 91058 Erlangen, Germany.

b Department of Chemistry, University of Alberta, 11227 Saskatchewan Drive, Edmonton, Alberta, Canada T6G 2G2.

c Department of Chemistry and Pharmacy & Computer-Chemie-Center (CCC), Friedrich-Alexander-Universität Erlangen-Nürnberg, Nägelsbachstr. 25, 91052 Erlangen, Germany.

† These authors contributed equally.

* Corresponding authors

KEYWORDS: singlet fission, up-conversion, tetracene, light harvesting, down-conversion

ABSTRACT: Photon energy conversion can be accomplished in many different ways, including the two opposing manners, down-conversion (i.e., singlet fission, SF) and up-conversion (i.e., triplet-triplet annihilation up-conversion, TTA-UC). Both processes have the potential to help overcome the detailed balance limit of single-junction solar cells. Tetracene, in which the energies of the lowest singlet excited state and twice the triplet excited state are comparable, exhibits both down- and up-conversion. Here, we have designed *meta*-diethynylphenylene- and 1,3-diethynyladamantyl-linked tetracene dimers, which feature different electronic coupling, to characterize the interplay between intramolecular SF (intra-SF) and intramolecular TTA-UC (intra-TTA-UC) via steady-state and time-resolved absorption and fluorescence spectroscopy. Furthermore, we have used Pd-phthalocyanine as a sensitizer to enable intra-TTA-UC in the two dimers via indirect photoexcitation in the near-infrared part of the solar spectrum. The work is rounded off by temperature-dependent measurements, which outline key aspects of how thermal effects impact intra-SF and intra-TTA-UC in the different dimers.

Introduction

Solar energy is essential if an ever-increasing demand for energy is to be satisfied. While abundant, the solar radiation reaching the earth's surface covers a broad range of energies, from high-energy ultraviolet, through the visible region, to low-energy infrared.[1,2] Efficient solar energy capture and conversion are, therefore, challenging. For photons with energies well-above the band-gap of the absorbing material, excess energy is lost predominantly as heat. In contrast, photons with energies below the optical band-gap are not absorbed at all.[3] Therefore, single-junction solar cells are limited to a maximum performance of 33% known as the detailed balance limit.[4] Both down- and up-conversion have the potential to increase solar-energy conversion efficiencies beyond current limitations.[5,6,7,8,9,10]

Singlet fission (SF), a down-conversion process, describes the splitting of one singlet exciton into a pair of triplet excitons after the absorption of a high-energy photon.[9,11,12] SF is spin-allowed and fast, as the correlated triplet pair $^1(T_1T_1)$ is of overall singlet multiplicity. To date, several SF mechanisms have been reported, and, in general, these studies describe either an incoherent or coherent process for SF.

Considering the incoherent scenario, one differentiates between a direct and a two-step mechanism. If coupling between (S_1S_0) and $^1(T_1T_1)$ is strong, $^1(T_1T_1)$ will evolve directly from (S_1S_0).[12,13,14,15,16] In the two-step mechanism, SF proceeds via an intermediate state that mediates the coupling between (S_1S_0) and $^1(T_1T_1)$.[17,18,19,20,21] The intermediate is usually a charge transfer (CT) state, and depending on the relative energy of the CT state with respect to (S_1S_0) and $^1(T_1T_1)$, it acts as either a real (observable) intermediate or as a virtual state. This case is often referred to the superexchange mechanism. If the energy of the CT state drops significantly below that of either (S_1S_0) or $^1(T_1T_1)$ it is likely to be a trap, and, in turn, the formation of $^1(T_1T_1)$ does not occur as direct recovery of the ground state dominates.[22,23]

When turning to the coherent scenario, a superposition of (S_1S_0), $^1(T_1T_1)$, and the CT state is formed upon photoexcitation.[13,24,25,26,27,28,29,30] Strong mixing between all three of states is realized if the energetic differences are small. The composition of the coherent superposition changes as a function of time, and different products evolve as a result of dephasing. Such products range from excimers to symmetry-breaking charge-separated states and $^1(T_1T_1)$.

SF would not be complete without the decoherence of $^1(T_1T_1)$, which generates two independent triplet excited states ($T_1 + T_1$). Decoherence requires a weakening of the coupling between the two triplet excited states in $^1(T_1T_1)$.[31,32,33] En-route towards ($T_1 + T_1$) the quintet form of the correlated triplet pair $^5(T_1T_1)$ is the key intermediate.[12,18,34,35] Time-resolved electron paramagnetic resonance (TREPR) is essential to corroborate the involvement of $^5(T_1T_1)$.[18,34,36,37] Comprehension of the decoherence is linked to the $^1(T_1T_1)$-$^5(T_1T_1)$ energy gap. Per se, electronic interactions between the two triplet excited states in $^5(T_1T_1)$ are weaker than in $^1(T_1T_1)$. This energy difference defines the binding energy, which needs to be overcome for the transformation of $^1(T_1T_1)$ to ($T_1 + T_1$).[38,39] In the strong coupling regime, exchange interactions are large and suppress $^1(T_1T_1)$-$^5(T_1T_1)$ mixing.[12,13,34] Consequently, the two triplet excited states remain bound. In the weak coupling regime, mixing of $^1(T_1T_1)$-$^5(T_1T_1)$ is feasible,[31,34,38] and electronic coupling takes place, albeit both triplet excited states will remain spin-entangled. Eventually, decoherence to produce ($T_1 + T_1$) is achieved via diffusion of the triplet excited states, interaction with the environment, or nuclear rearrangement.[11,18,34]

The thermodynamic requirement for SF necessitates that the energy of the first singlet excited state (S_1) must exceed, or at least approximate, twice that of the first triplet excited state (T_1). Exothermic SF, such as observed in pentacene, is typically fast and efficient,[17,40,41] while the energy barrier for triplet-triplet annihilation up-conversion (TTA-UC), the reverse process, renders the fusion of the resulting triplet excitons to produce (S_1S_0) unfavorable. Such an exoergic process comes, however, at the expense of thermal losses that lead to overall inefficient solar energy conversion. Furthermore, low triplet excited state energies complicate use in, for example, photovoltaics. Conversely, materials that feature isoergic or slightly endergonic SF, such as tetracene, are suitable for emerging applications.[42,43] Notably, if SF is isoergic, dissociation of the correlated triplet pair into free triplet excited states may be hindered by thermally activated triplet-triplet annihilation up-conversion (TTA-UC), a competitive process that yields a higher-lying singlet excited state.[44,45,46,47]

TTA-UC is the reverse process to SF and involves the fusion of two low-energy triplet excited states to provide one high-energy singlet excited state.[48,49,50,51] For TTA-UC to occur, the energy of the singlet excited state of the annihilator must be lower than twice the energy of the triplet excited state. Based on this parameter, polycyclic aromatic hydrocarbons, including anthracene,[52,53,54] tetracene,[55,56,57] perylene,[58,59,60] and their derivatives have been explored as annihilators in combination with triplet sensitizers that undergo photoexcitation at long wavelengths. TTA-UC is typically a diffusion-controlled, bimolecular process, and photo-sensitized TTA-UC measurements are typically conducted in the high-concentration regime. Seminal work on TTA-UC using dimeric and oligomeric annihilators confirms that intramolecular TTA-UC (intra-TTA-UC) helps to circumvent the need for high concentrations.[54,55,57,61] On the other hand, a definitive scheme describing the process of intra-TTA-UC and how it affects the efficiency of TTA-UC is still lacking.

Intramolecular SF (intra-SF) in molecular dimers and oligomers is at the forefront of recent investigations of this process. For dimers, the fate of $^1(T_1T_1)$ is governed by the electronic coupling between the two chromophores.[18,31,33,34] Control over the coupling is realized by different spacer motifs. In strongly coupled dimers, $^1(T_1T_1)$-$^5(T_1T_1)$ mixing is impossible and $^1(T_1T_1)$ deactivates via fast TTA. In contrast, weakly coupled dimers allow for $^1(T_1T_1)$-$^5(T_1T_1)$ mixing and subsequent decoherence to produce ($T_1 + T_1$) (an essential event for effective SF). Considering that the initial product of intra-SF, namely $^1(T_1T_1)$, bears two coupled triplet excited states, $^1(T_1T_1)$ is a promising starting point to

investigate intra-TTA-UC. Thus, fine-tuning of the electronic coupling by means of different spacer motifs allows for investigating the interplay between the intertwined processes of SF and TTA-UC. Importantly, this becomes imperative in the design of advanced materials.

Acenes – such as anthracene, tetracene, pentacene - and their derivatives are widely used as building blocks to probe multiexcitonic processes like SF and TTA-UC. In anthracene and pentacene, the energy of (S_1) is lower or higher than twice the energy of (T_1), respectively, which renders them suitable for the individual investigation of either TTA-UC or SF, respectively. In contrast, the (S_1) energy of tetracene is close to twice the energy of (T_1), and both SF and TTA-UC are thermodynamically feasible.[62] Previous investigations have documented that tetracene is indeed capable of undergoing inter- and intramolecular SF[46,47,63,64,65] and TTA-UC.[55,56,57,66] To the best of our knowledge, however, studies regarding the interplay between SF and TTA-UC remain rare. To unravel the interplay between SF and TTA-UC, rigidly linked tetracene dimers are a promising platform as they allow for the control of electronic coupling by synthetic design.[63,64,67,68,69]

In analogy to our previous work on intra-SF in pentacene dimers,[34,67,70] we designed two covalently linked tetracene dimers that are rigidly bridged by either a cross-conjugated *meta*-diethynylphenylene (**mPhTc$_2$**) or a non-conjugated 1,3-diethynyladamantyl spacer (**mAdTc$_2$**). Importantly, the through-bond electronic coupling is dictated by the spacer, while the geometrical and spatial arrangements remain nearly identical. Intra-SF and intra-TTA-UC are unequivocally demonstrated for **mPhTc$_2$** and **mAdTc$_2$** through a combination of steady-state and time-resolved measurements. Using Pd(II) 1,4,8,11,15,18,22,25-octabutoxyphthalocyanine (**PdPc**) as the photosensitizer, we find that both **mPhTc$_2$** and **mAdTc$_2$** give rise to more efficient TTA-UC than the corresponding monomers **PhTc** and **AdTc**, confirming the intramolecular nature of TTA-UC. In particular, **mPhTc$_2$** shows the highest UC efficiency regardless of the concentration. Our results underpin the significance of inter-chromophore electronic coupling in intra-SF and intra-TTA-UC as we highlight the opposing dependencies of intra-SF and intra-TTA-UC on the inter-chromophore coupling and provide a crucial guideline for designing molecules that feature either efficient dissociation of $^1(T_1T_1)$ or efficient up-conversion from $^1(T_1T_1)$ via TTA-UC.

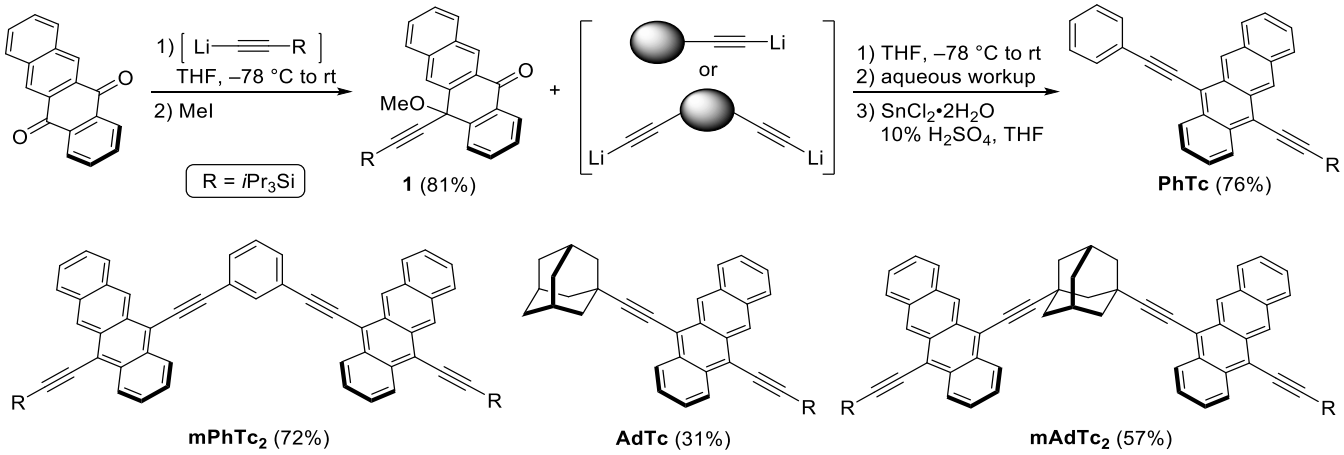

Scheme 1. Synthesis of tetracene dimers **mPhTc$_2$** and **mAdTc$_2$** as well as the corresponding monomers **PhTc** and **AdTc**.

Results and Discussion

Synthesis The cross-conjugated and non-conjugated tetracene dimers **mPhTc$_2$** and **mAdTc$_2$** and the corresponding tetracene monomers **PhTc** and **AdTc** were synthesized through a stepwise substitution of 5,12-naphthacenequinone by adapting protocols used to form tetracene[71] and pentacene dimers (Scheme 1).[34,72] Briefly, addition of lithiated tri*iso*propylsilylacetylene (*i*Pr$_3$Si–C≡C–Li) to a suspension of 5,12-naphthacenequinone in dry tetrahydrofuran (THF) at –78 °C followed by in situ trapping of the resulting alkoxide with MeI affords the common building block **1**. Nucleophilic addition of a lithiated mono- or diyne to ketone **1**, followed by $SnCl_2$-mediated reductive aromatization produced the desired products. The products were purified by column chromatography and isolated in acceptable to good yield as scarlet solids. The structures of **PhTc** and **mPhTc$_2$** are confirmed by X-ray crystallography (Supporting Information).

Intramolecular Electronic Coupling The four tetracene derivatives were probed by quantum chemical calculations and steady-state absorption spectroscopy in different solvents to characterize the impact of the spacer on intramolecular interactions in the ground state. We used two different configuration interaction (CI) expansions to investigate different aspects of the systems. AM1 UNO-CIS calculations (Supporting Information) are the most suited for calculating energies of excited states, but only give information on singlet and triplet states because they only include single excitations from the ground state. They show that S^1 (2.457 eV, 504.7 nm) in **AdTc** becomes S^1 and S^2 (2.424 and 2.486 eV, 511.4 and 498.7 nm) in **mAdTc$_2$**. S^1 and S^2 are separated by 0.062 eV in **mAdTc$_2$**, compared to 0.128 eV in **mPhTc$_2$** because of stronger electronic coupling between the tetracene moieties in **mPhTc$_2$**.[73] AM1-CISD

calculations (Supporting Information) were used to investigate coupling between the various (T_1T_1) states of different multiplicity because the extra doubly excited states used in the calculation allow for states of higher multiplicity to be observed than in the CIS calculations. However, these doubly excited states stabilize the ground state strongly and lead to calculated excitation energies that are too high. Nonetheless, energy differences between the states of interest are reliable. For AM1-CISD, the dependence of coupling on the spacer was demonstrated by calculating the splitting between different spin multiplicities of (T_1T_1), namely, $^1(T_1T_1)$, $^3(T_1T_1)$, and $^5(T_1T_1)$. In **mAdTc$_2$**, these three states all occur at the same energy (4.022 eV),[74] which is 0.34 and 0.27 eV above the strongly absorbing S^1 (3.680 eV at AM1-CISD) and S^2 (3.752 eV at AM1-CISD) states, respectively. In contrast, the calculated excitation energies in **mPhTc$_2$** are 4.065, 4.066, and 4.108 eV for the $^1(T_1T_1)$, $^3(T_1T_1)$, and $^5(T_1T_1)$ states, respectively. $^1(T_1T_1)$ in **mPhTc$_2$** is 0.39 and 0.26 eV higher in energy than S^1 (3.679 eV at AM1-CISD) and S^2 (3.806 eV at AM1-CISD), respectively. The splitting between $^1(T_1T_1)$ and $^5(T_1T_1)$ is 0.04 eV in **mPhTc$_2$**, confirming the hypothesis that inter-chromophore coupling is stronger in **mPhTc$_2$** than in **mAdTc$_2$**.[33] This is entirely consistent with the cross-conjugated π-system linking the chromophores in **mPhTc$_2$** with coupling caused by electronic delocalization, compared to the "insulating" alkane-like path in **mAdTc$_2$**. Note that AM1 UNO-CIS calculations[75] have proven to be very reliable for excitation energies in general, and that AM1-CISD successfully treats the splitting of "equivalent" singlet, triplet and quintet states,[17] so that we expect the results to be reliable.

At first glance, similar steady-state absorption spectra are found for all four derivatives in both toluene and benzonitrile (Figures 1 and S11 and Table S2). In particular, high-energy (300–400 nm) transitions to populate higher singlet excited states go hand-in-hand with low-energy transitions (450–600 nm) to populate the first singlet excited state. Distinct vibrational fine structure involving the transitions 0-*0, 0-*1, 0-*2, etc., is observed in the region of 450–600 nm. In toluene, for example, **AdTc** displays absorption maxima at 464, 496, and 533 nm. The absorption features of **PhTc** are shifted bathochromically by 0.047 eV in comparison to **AdTc** and show slightly higher extinction coefficients as a result of extended π-conjugation and better electronic delocalization. More significant differences are observed when comparing the steady-state absorption spectra of the dimers **mAdTc$_2$** and **mPhTc$_2$**. The spectrum of **mAdTc$_2$** represents a linear sum of two **AdTc** monomers, both in terms of absorption maxima and extinction coefficients. For **mPhTc$_2$**, the absorption maxima are further redshifted than for **PhTc** and the spectrum does not represent the linear sum of two **PhTc** monomers. To be precise, the intensity ratios of the vibronic peaks ($I_{0\text{-}*0}/I_{0\text{-}*1}$) are 1.58 and 1.41 for **mPhTc$_2$** and **PhTc**, respectively in toluene. These observations confirm that the intramolecular electronic coupling is appreciably stronger in **mPhTc$_2$** than in **mAdTc$_2$**.

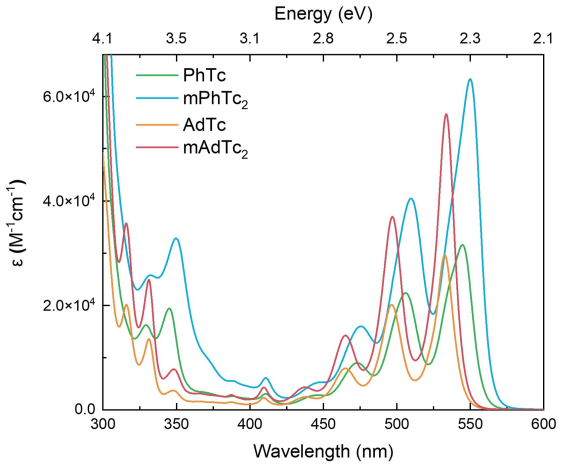

Figure 1. Room-temperature steady-state absorption spectra of **PhTc** (green), **mPhTc$_2$** (blue), **AdTc** (orange), and **mAdTc$_2$** (red) in toluene.

Intramolecular Down-conversion Femtosecond and nanosecond transient absorption spectroscopy (fs-TAS and ns-TAS) have been performed based on photoexcitation at 480 nm. The singlet excited state (S_1) of the monomer **PhTc** in toluene forms immediately after photoexcitation and is characterized by a dominant, excited-state absorption (ESA) in the range of 400–500 nm, a sharp ground-state bleaching (GSB) overlaid with stimulated emission (SE) from 500–600 nm and a broad ESA in the 800–1400 nm range (Figure 2). Essentially the same features evolve for (S_1) of monomer **AdTc** on the fs-TAS timescale (Figure S12). Raw data from fs-TAS experiments of **PhTc** and **AdTc** are best fit by Global Analysis with a sequential kinetic model based on two species (Figures 2 and S12-14). On this basis, we assign these two species as (S_1) and $(S_1)_{rel}$, namely (S_1) before and after relaxation to the minimum of the (S_1) potential energy surface via structural relaxation and solvent reorganization. In contrast to the spectroscopic features, which are independent of solvent polarity, the lifetime of (S_1), varies as a function of solvent (Table 1). In benzonitrile, the lifetimes are 86.0 ps for **PhTc** and 207.4 ps for **AdTc**, while they are dramatically reduced to 2.7 ps for **PhTc** and 121.5 ps for **AdTc** in toluene. We rationalize this observation by the greater viscosity of benzonitrile, which slows down structural relaxation and solvent reorganization. The differences between **PhTc** and **AdTc** stem from the lower structural flexibility of **PhTc** due to π-conjugation. Once formed, $(S_1)_{rel}$ decays predominantly via fluorescence with a quantum yield of around 70% for both monomers(*vide infra*). As the timescale of fs-TAS is insufficient to cover the full decay dynamics of $(S_1)_{rel}$ for **PhTc** and **AdTc**, we turned to ns-TAS (Figures 3 and S15-S17). In the case of **PhTc**, (S_0) is quantitatively reinstated with a lifetime of ca. 10 ns (Table 1), which is in line with time-correlated single-photon counting (TCSPC) measurements (*vide infra*). In stark contrast, $(S_1)_{rel}$ deactivation for **AdTc** is linked to the formation of another state that persists on the timescale of microseconds. This newly formed state is consistent with that generated in triplet-triplet sensitization measurements using *N*-methylfulleropyrrolidine (***N*-MFP**) as a photosensitizer

with photoexcitation at 387 nm. (Figures S18 and S20). Thus, we assign it to the first triplet excited state (T_1) of **AdTc**. In light of the high fluorescence quantum yield (70%), however, it is clear that only a small fraction of $(S_1)_{rel}$ is transformed to (T_1) via slow spin-forbidden intersystem crossing (ISC).

The picture is quite different for covalent dimers **mPhTc$_2$** and **mAdTc$_2$**. For both dimers, three rather than two species are required to fit the fs-TAS data by means of Global Analysis employing a sequential kinetic model (Figures 4, S21-S23). The characteristics of the first and second species are assigned as singlet excited states before (S_1S_0) and after relaxation $(S_1S_0)_{rel}$, respectively, consistent with (S_1) and $(S_1)_{rel}$ as observed for monomers **PhTc** and **AdTc**. ESAs between 400–500 and 600–1400 nm next to GSB in the range of 500–600 nm corroborate this assignment.[76] The lifetime of $(S_1S_0)_{rel}$ depends on both spacer and solvent (Table 1). For **mPhTc$_2$**, the lifetimes of $(S_1S_0)_{rel}$ are 46.9 ps in benzonitrile and 80.0 ps in toluene, respectively, while they are significantly longer for **mAdTc$_2$** with 369.1 ps and 886.6 ps in benzonitrile and toluene, respectively. The third species is characterized by attenuated broad singlet ESAs in the range of 600–1400 nm along with triplet ESAs at 523 nm for **mPhTc$_2$** and 502 nm for **mAdTc$_2$** (*vide infra*). The fact that the triplet-excited state signatures appear within hundreds of picoseconds indicates that population of the triplet excited-state occurs via fast spin-allowed intra-SF rather than slow spin-forbidden intersystem crossing (ISC). The evolution of the triplet excited-state features is more rapid for **mPhTc$_2$** than for **mAdTc$_2$** and demonstrates that intra-SF is faster in **mPhTc$_2$** than in **mAdTc$_2$**. This is attributed to the stronger electronic coupling in **mPhTc$_2$** due to the π-conjugation of the spacer. In **mAdTc$_2$** the non-conjugated 1,3-diethynyladamantyl spacer reduces the inter-tetracene coupling significantly. Of great relevance is the signature of **mPhTc$_2$** in benzonitrile in the range of 800–1100 nm, which matches the absorption spectrum of the one-electron oxidized form of **mPhTc$_2$** obtained via chemical oxidation (Figure S24). The agreement for **mPhTc$_2$** in benzonitrile is particularly good, and the CT signatures are clearly discernable in this case. Indications of CT are, however, inconspicuous for **mPhTc$_2$** in toluene, and they are not observed for **mAdTc$_2$**, even in polar benzonitrile, as a result of weaker electronic coupling in **mAdTc$_2$**. Therefore, we conclude that the evolution associated spectrum (EAS) of the third species bears contributions from the singlet and triplet excited state as well as from a CT state. As expected, the contribution of the CT state strongly depends on the nature of the spacer and the solvent polarity. In line with our recent work on pentacene dimers,[30] and the work from Wasielewski and co-workers on terylenediimide dimers,[27,28,29] we postulate that the third species is a superposition of $(S_1S_0)_{rel}$, the CT state, and $^1(T_1T_1)$ to give a mixed state which we refer to as $(S_1S_0)_{(T1T1)^{CT}}$.

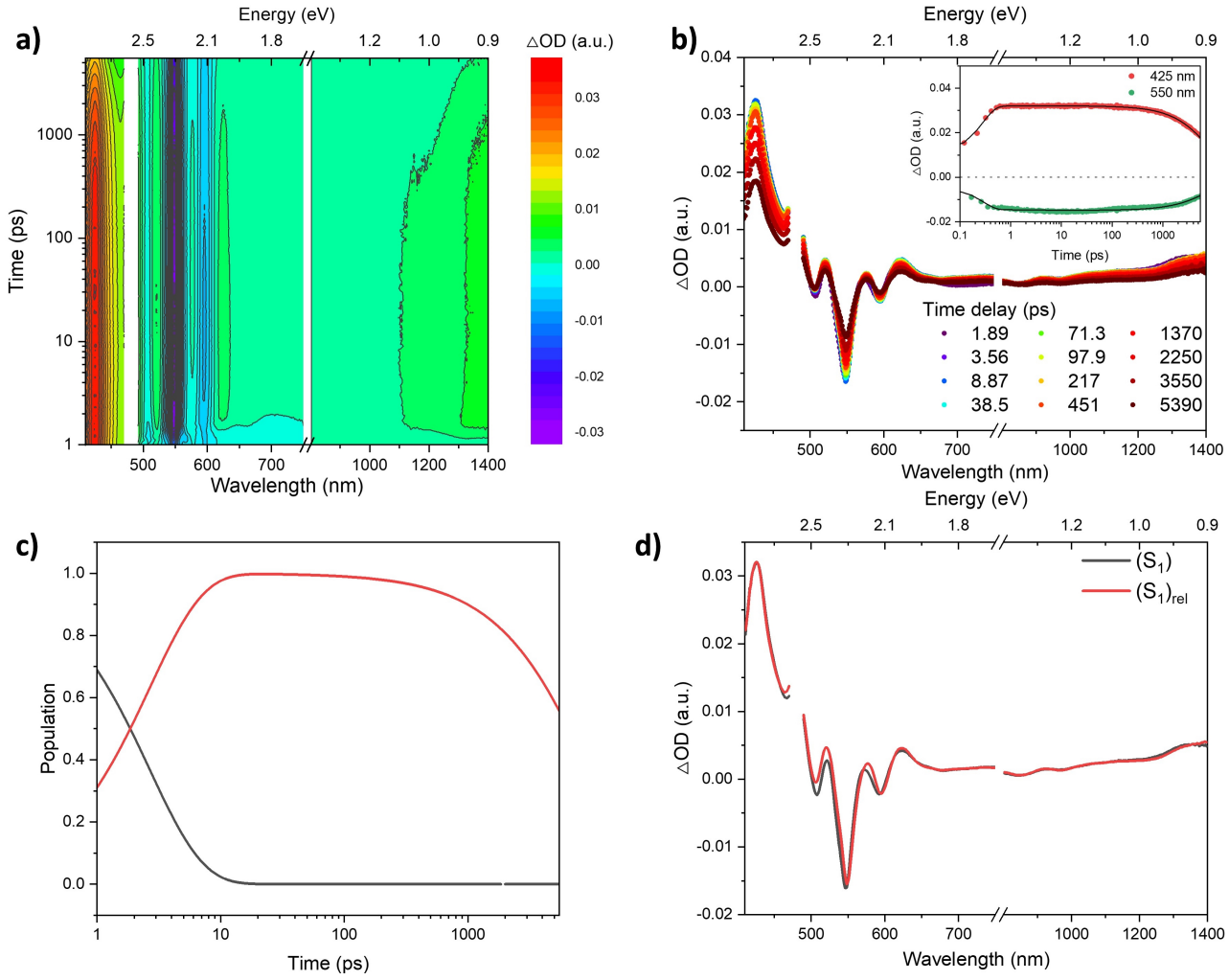

Figure 2. Global Analysis of the fs-TAS raw data for **PhTc** following photoexcitation at 480 nm in argon-saturated toluene at room temperature. a) Heat map of fs-TAS raw data obtained from pump-probe experiments with time delays up to 5500 ps. b) Differential absorption spectra at various time delays. Insert: Time absorption profiles as well as corresponding fits of selected wavelengths (see the figure legend for details). c) Relative populations of the respective species with colors correlating with the evolution associated spectra (EAS). d) EAS of the deconvoluted species: the first species is the singlet excited state (S_1) (grey), and the second species is the relaxed singlet excited $(S_1)_{rel}$ (red); note that $(S_1)_{rel}$ cannot be completely deconvoluted on this timescale.

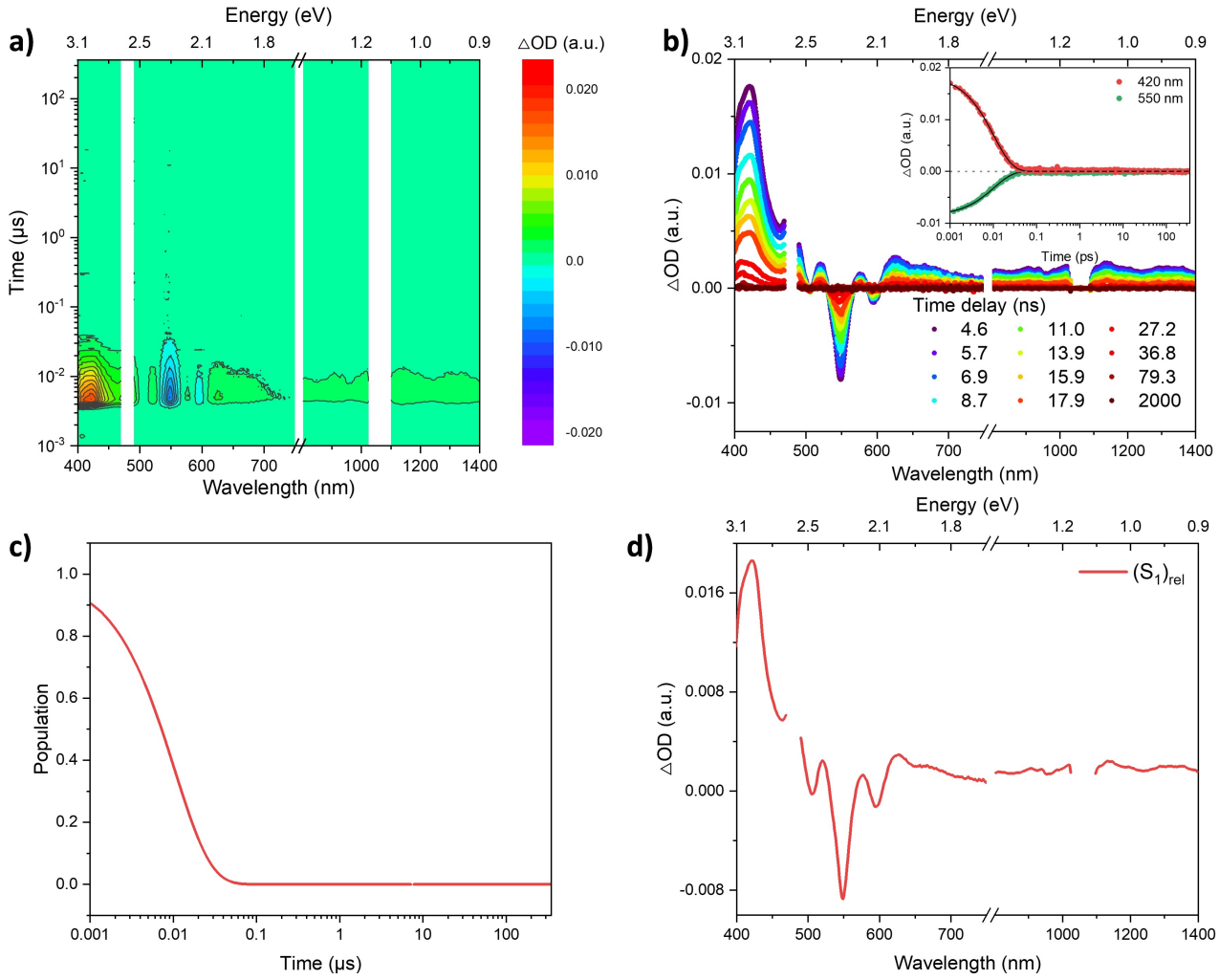

Figure 3. Global Analysis of the ns-TAS raw data for **PhTc** following photoexcitation at 480 nm in argon-saturated toluene at room temperature. a) Heat map of ns-TAS raw data obtained from pump-probe experiments with time delays up to 350 μs. b) Differential absorption spectra at various time delays. Insert: Time absorption profiles as well as corresponding fits of selected wavelengths (see the figure legend for details). c) Relative populations of the respective species with colors correlating with the evolution associated spectra (EAS). d) EAS of the deconvoluted species: relaxed singlet excited state (S1)rel (red).

The fate of $(S_1S_0)_{(T1T1)}{}^{CT}$ was determined in ns-TAS measurements. Global Analysis based on a sequential kinetic model with three species fits the ns-TAS raw data of both **mPhTc₂** and **mAdTc₂**. (Figures 5 and S25–S27). Importantly, the third fs-TAS species and the first ns-TAS species are both the intermediate state $(S_1S_0)_{(T1T1)}{}^{CT}$. The lifetime of $(S_1S_0)_{(T1T1)}{}^{CT}$ is ca. 10 ns and is barely affected by solvent polarity and spacer (Table 1). The second and third species share the same spectral signatures, that is ESA at 502 nm along with GSB at 535 nm for **mPhTc₂**, and ESA at 523 nm as well as GSB at 550 nm for **mAdTc₂** in toluene. To establish their identity, triplet-triplet sensitization measurements were performed, using *N*-methylfulleropyrrolidine (***N*-MFP**) as the photosensitizer, with photoexcitation at 387 nm (Figures S18, S28, and S29). The spectral similarities between the sensitized (T_1) and the spectroscopic signatures of both the second and third species in the ns-TAS are striking. We conclude that two different triplet excited states are formed for both **mPhTc₂** and **mAdTc₂**. The lifetimes of the two different triplet species are 66.5 ns and 51.1 μs in toluene for **mPhTc₂** and 73.7 ns and 90.0 μs for **mAdTc₂**. The fact that the triplet ESAs of both dimers decay bi-exponentially, instead of mono-exponentially as seen for the monomer **AdTc**, is further evidence that a different mechanism, namely intra-SF, is responsible for the triplet excited-state population of **mPhTc₂** and **mAdTc₂**. Thus, we assign the second species to the correlated triplet pair (T_1T_1), which has been formed directly from $(S_1S_0)_{(T1T1)}{}^{CT}$ via fast spin-allowed intra-SF. To be precise, formation of (T_1T_1) occurs upon dephasing of $(S_1S_0)_{(T1T1)}{}^{CT}$, induced by nuclear rearrangement or solvent relaxation. The third species, whose lifetime is fully consistent with any microsecond-lived free (T_1), as observed for **AdTc**, is ascribed to uncorrelated triplet excited state ($T_1 + T_1$) that is from decoherence of (T_1T_1).

Notably, the final step of intra-SF, that is (T_1T_1) decoherence to produce two independent triplet excited states (T_1+T_1), is observed in both strongly coupled **mPhTc$_2$** and weakly coupled **mAdTc$_2$**. The quintet form of (T_1T_1), namely ^{5}(T_1T_1), is an intermediate along the dissociation of ^{1}(T_1T_1) in dimeric systems.[12,18,34,35] The deconvolution of ^{1}(T_1T_1) and ^{5}(T_1T_1) failed as both states are indistinguishable by means optical spectroscopy. Thus, we refer to (T_1T_1) rather than ^{1}(T_1T_1) or ^{5}(T_1T_1).[18] The short lifetime of (T_1T_1), especially for **mPhTc$_2$**, suggests that TTA is active. As a matter of fact, TTA represents a competitive deactivation pathway to the decoherence of (T_1T_1).[46,77]

.

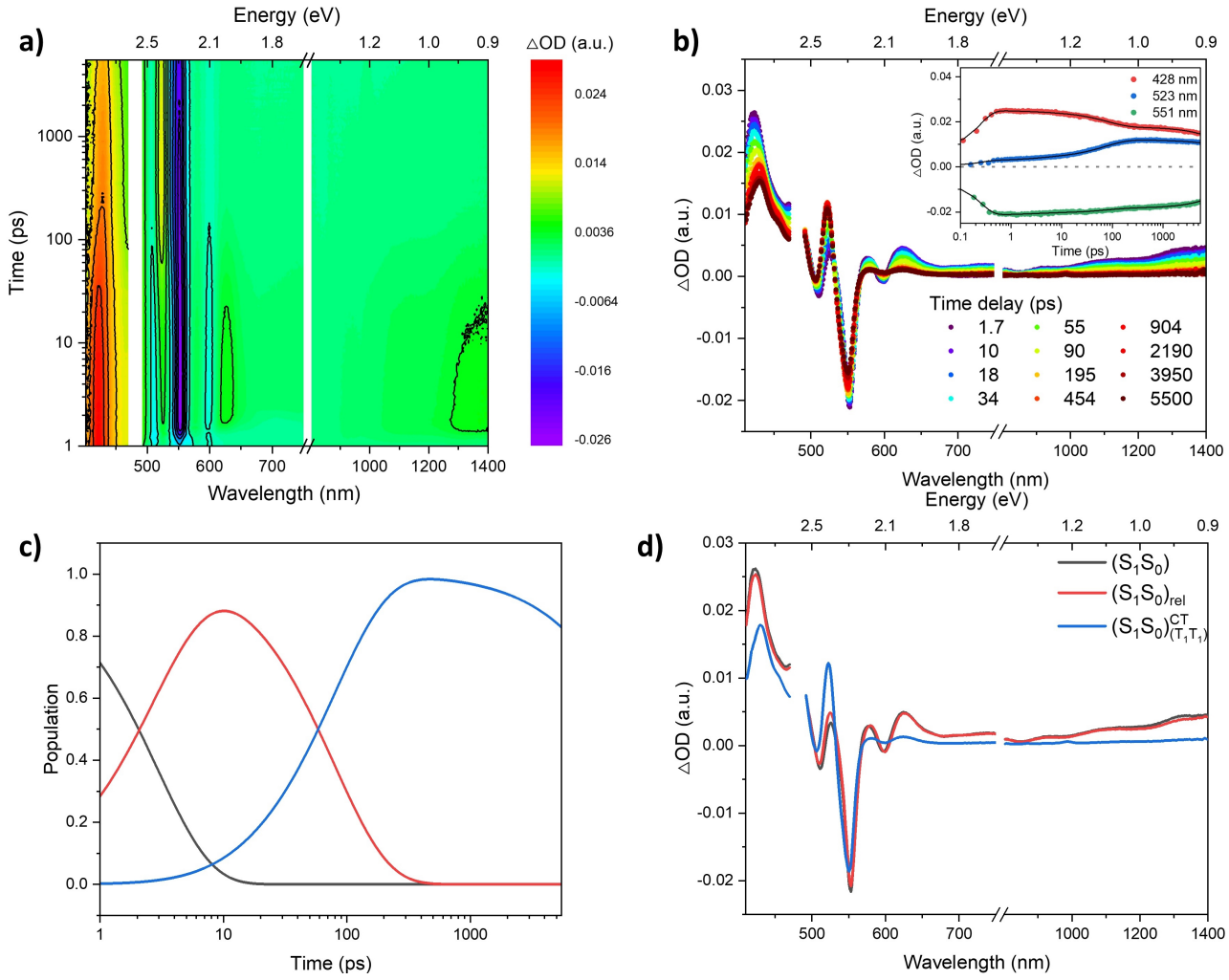

Figure 4. Global Analysis of the fs-TAS raw data for **mPhTc$_2$** following photoexcitation at 480 nm in argon-saturated toluene at room temperature. a) Heat map of fs-TAS raw data obtained from pump-probe experiments with time delays up to 5500 ps. b) Differential absorption spectra at various time delays. Insert: Time absorption profiles as well as corresponding fits of selected wavelengths (see the figure legend for details). c) Relative populations of the respective species with colors correlating with the evolution associated spectra (EAS). d) EAS of the deconvoluted species: the first species is the singlet excited state (S_1S_0) (grey), the second species is the relaxed singlet excited state $(S_1S_0)_{rel}$ (red), and the third species is the intermediate state $(S_1S_0)_{(T1T1)}{}^{CT}$ (blue); note that $(S_1S_0)_{(T1T1)}{}^{CT}$ is not completely deconvoluted on this timescale.

Triplet quantum yields (Φ_T) for **mPhTc$_2$** and **mAdTc$_2$** have been approximated by means of singlet oxygen quantum yields (Φ_Δ) (Supporting Information and Table 1). The (T_1) energy of tetracene (1.21 eV) is higher than those of pentacene and molecular oxygen with ca. 0.8 and 0.98 eV, respectively. Hence, diffusive triplet-triplet energy transfer (TTEnT) from tetracene and O_2 is thermodynamically feasible.[55,78] For both **mPhTc$_2$** and **mAdTc$_2$**, all values of Φ_Δ exceed 100%, which is an unambiguous indication for intra-SF. Values of Φ_Δ are as high as 170% for **mAdTc$_2$** and 128% for **mPhTc$_2$** in toluene. It is noted that a faster intramolecular TTA impacts Φ_Δ. In particular, stronger electronic coupling in **mPhTc$_2$** favors (T_1T_1) deactivation via TTA prior to any collision with O_2. Consequently, lower Φ_Δ values evolve for **mPhTc$_2$** than for **mAdTc$_2$**. Furthermore, Φ_Δ values for both dimers are higher in toluene than in more polar benzonitrile. We rationalize this trend by considering two aspects. On one hand, the lower viscosity of toluene relative to benzonitrile allows for better diffusion and, therefore, more efficient sensitization of singlet oxygen. On the other hand, CT states are well known to be stabilized in polar solvents like benzonitrile. Changing the energy of the CT state will change the composition of $(S_1S_0)_{(T1T1)}{}^{CT}$. Efficient mixing requires that the involved states are close in energy. SF is, however, slightly endothermic in tetracene. As such, it is likely that a lower-energy CT state will mix preferably with $^1(S_1S_0)$ rather than with (T_1T_1). In other words, the contribution of (T_1T_1) to $(S_1S_0)_{(T1T1)}{}^{CT}$ will be lower in a more polar solvent. The consequence of reduced mixing of (T_1T_1) to the coherent superposition will hamper intra-SF and, in turn, reduce Φ_Δ in more polar solvents. A dependence of Φ_Δ on solvent polarity is taken as further evidence for the participation of a CT state in intra-SF.

Finally, the yields for the dissociation of (T_1T_1) to afford uncorrelated triplet excited states (T_1 + T_1) have been determined (Tables 1 and S3). This analysis was aided by the fact that the GSB and triplet ESA related extinction

coefficients remain constant throughout the dissociation process. Therefore, the dissociation yield can be calculated using the ratio between the ΔOD values of the EAS of (T_1T_1) and (T_1 + T_1). The dissociation yield (Φ_{Diss}) for **mAdTc$_2$** in benzonitrile (46%) is 10-times greater than that for **mPhTc$_2$** (4.5%). It is noted that high values of Φ_{Diss} were found in pentacene dimers with a 1,3-diethynyladamantyl spacer, while dimers with a 1,3-diethynylphenylene spacer fail to produce significant amounts of (T_1 + T_1).[34,70] In line with quantum chemical calculations, weak electronic coupling in **mAdTc$_2$** favors ^{1}(T_1T_1)-^{5}(T_1T_1) spin-mixing and allows for dissociation of (T_1T_1) to form (T_1 + T_1). Stronger inter-tetracene coupling in **mPhTc$_2$** lifts the degeneracy of ^{1}(T_1T_1) and ^{5}(T_1T_1) and, therefore, inhibits ^{1}(T_1T_1)-^{5}(T_1T_1) mixing. Consequently, (T_1T_1) dissociation is very unlikely in **mPhTc$_2$**.

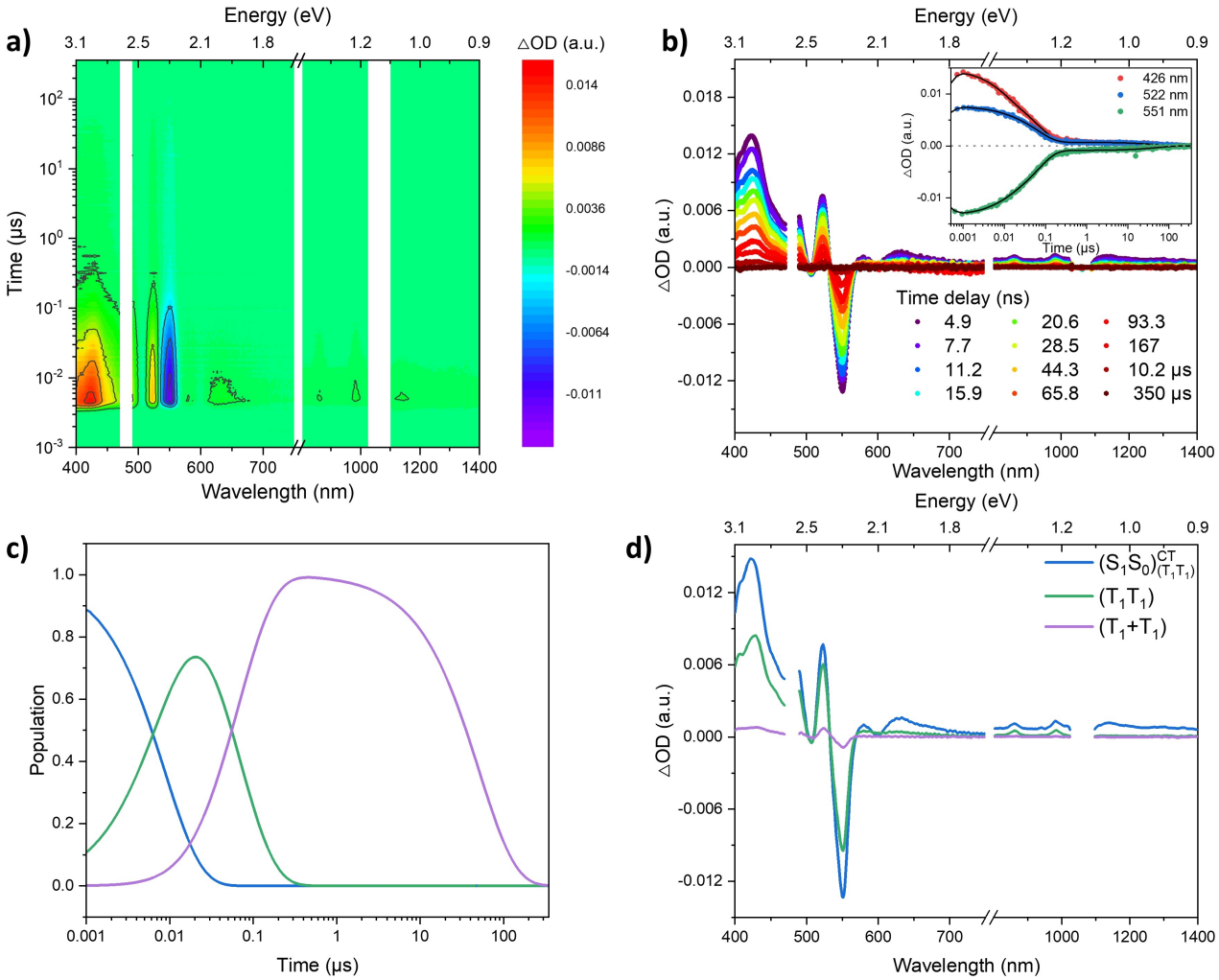

Figure 5. Global Analysis of the ns-TAS raw data for **mPhTc$_2$** following photoexcitation at 480 nm in argon-saturated toluene at room temperature. a) Heat map of ns-TAS raw data obtained from pump-probe experiments with time delays up to 350 µs. b) Differential absorption spectra at various time delays. Insert: Time absorption profiles as well as corresponding fits of selected wavelengths (see the figure legend for details). c) Relative populations of the respective species with colors correlating with the evolution associated spectra (EAS). d) EAS of the deconvoluted species: the first species is the intermediate state $(S_1S_0)_{(T1T1)}{}^{CT}$ (blue), the second species is the correlated triplet pair (T_1T_1) (green), and the third species represents two uncorrelated triplet excited states (T_1 + T_1) (violet)

Table 1. Lifetimes (τ) and dissociation quantum yields (Φ_{Diss}) obtained from Global Analysis of fs- and ns-TAS, as well as singlet oxygen quantum yields (Φ_{Δ}) of **AdTc**, **PhTc**, **mAdTc$_2$**, and **mPhTc$_2$** in toluene (Tol) and benzonitrile (BN).

		fs-TAS		ns-TAS				
	Solvent	(S_1S_0) (ps)	$(S_1S_0)_{rel}$ (ps)	$(S_1S_0)_{CT}^{(T1T1)}$ (ns)	(T_1T_1) (ns)	(T_1+T_1) (µs)	Φ_{Δ} [a]	Φ_{Diss} [b]
AdTc	BN	207.4	14.0	-	-	76.0	-	-
	Tol	121.5	14.8	-	-	39.6	-	-
PhTc	BN	86.0	10.3	-	-	-	-	-
	Tol	2.7	10.4	-	-	-	-	-
mAdTc$_2$	BN	7.5	369.1	12.5	78.1	290.6	113.2%	46.1%
	Tol	6.2	886.6	8.9	73.7	90.0	170.0%	45.9%
mPhTc$_2$	BN	-	46.9	9.0	39.5	77.5	101.9%	4.5%
	Tol	2.9	80.0	8.7	66.5	51.1	128.8%	9.0%

[a] Φ_{Δ} is determined using C_{60} in toluene as reference. An error margin of ±10% is implicit in the determination of Φ_{Δ}.
[b] Φ_{Diss}= $\Delta OD((T_1 + T_1))/\Delta OD((T_1T_1))$, where ΔOD refers to the ΔOD values of the ground state bleaching minimum of the evolution associated spectrum of the respective species. An error margin of ±10% is implicit in the determination of Φ_{Diss}.

Photosensitized Up-conversion In the next step, we probed **AdTc, PhTc, mAdTc$_2$, mPhTc$_2$** as annihilators in the context of photosensitized TTA-UC. To this end, we used a photosensitizer that generates (T_1) of the annihilator via TTEnT following low-energy excitation of the photosensitizer. Subsequently, two annihilators in their triplet excited states collide and undergo TTA-UC. The net result is one annihilator (S_0) and one annihilator (S_1) that fluoresces with higher energy. (Figure S32).[49] As such, the efficiency of TTA-UC ($\Phi_{UC\text{-}F}$) is given by

$$\Phi_{UC-F} = \frac{1}{2} f \Phi_{ISC} \Phi_{TTEnT} \Phi_{TTA} \Phi_F$$

where Φ_{ISC}, Φ_{TTEnT}, and Φ_{TTA}, are the efficiencies of ISC of the photosensitizer, TTEnT from the photosensitizer to the annihilator, and TTA of the annihilator, respectively, while Φ_F is the fluorescence quantum yield of the annihilator.[49,79] The parameter f is the spin statistical factor, which relates to the probability that (S_1) is formed upon TTA, and ½ is due to the fact that one high-energy photon is emitted upon absorption of two low-energy photons during TTA-UC.

Firstly, we examine the emission properties of the tetracene derivatives. The fluorescence spectra of the monomers and dimers upon photoexcitation at 480 nm are mirror images of the ground-state absorptions (Figure S33). The vibrational fine structure shows maxima at 535, 580, and 625 nm for both **AdTc** and **mAdTc$_2$** in toluene. These are redshifted to 550, 592, and 641 nm for **PhTc** and to 555, 597, and 643 nm for **mPhTc$_2$** as a result of extended π-conjugation. Under ambient conditions, **PhTc** and **AdTc** fluoresce strongly with quantum yields in the range of 70%, regardless of solvent polarity (Table S4). In contrast the fluorescence quantum yields of **mPhTc$_2$** and **mAdTc$_2$** are quenched to 6.9 and 15.6% in toluene, respectively, and to 21.3 and 19.6% in benzonitrile, respectively.

Secondly, the TTEnT dynamics were studied (Supporting Information). We used **PdPc** as triplet photosensitizer due to its near unity ISC efficiency, its high molar extinction coefficient of 1.8×10^5 $M^{-1}cm^{-1}$ at 730 nm, and the minimal spectral overlap between its absorption in the range of 600 to 800 nm and the tetracene fluorescence between 500 to 650 nm (Figure S35). Upon photoexcitation of **PdPc** at 730 nm in toluene, efficient intermolecular TTEnT (inter-TTEnT) from **PdPc** to the tetracene annihilators is confirmed via Stern-Volmer analyses, and the underlying inter-TTEnT rate constants are determined (k_{TTEnT}; Supporting Information). Considering (T_1) energies of 1.13 and 1.21 eV for **PdPc** and tetracene, respectively, inter-TTEnT is endergonic by +0.08 eV. All k_{TTEnT} values are within the same range of 10^9 $M^{-1}s^{-1}$ (Figure S36 and Table S5).

We next sought to establish TTA-UC as the subsequent step to TTEnT via photoexcitation of **PdPc** at 730 nm and recording the up-converted fluorescence from the tetracene derivatives annihilators in the range of 500–650 nm. **PdPc** and annihilator concentrations were held constant at 4.5×10^{-5} and 2.5×10^{-4} M, respectively. The power-law dependence of the integrated up-converted fluorescence intensity versus the incident photon power is the hallmark of TTA-UC. [79,80] At low incident power densities, some **PdPc** triplet excited states will not collide with an annihilation partner, but will decay non-radiatively. Under these conditions, the integrated up-converted fluorescence shows a quadratic dependence on the incident power density. At high incident power densities TTA-UC becomes dominant, and the dependence of up-converted fluorescence becomes linear. Importantly, the typical evolution from a quadratic to a linear power density dependence is observed for all up-conversion systems (Figure 6a) as the power is increased step-by-step, indicating that TTA-UC occurs. The crossing point, namely the power density threshold (I_{th}), is a key parameter for TTA-UC. At power densities above I_{th}, where the integrated up-converted fluorescence depends linearly on the power density, the TTA-UC efficiency reaches its maximum and remains constant. Therefore, low I_{th} values are desirable for effective utilization. The I_{th} values of **PhTc** and **AdTc** are 23.0 and 33.3 W/cm^2 respectively, while values as low as 9.5 and 16.0 W/cm^2 are realized using **mPhTc$_2$** and **mAdTc$_2$**, respectively. As **mPhTc$_2$** outperforms **mAdTc$_2$**, we optimized I_{th} further by increasing the concentration of **mPhTc$_2$**. As shown in Figure S37, an I_{th} value of 3.8 W/cm^2 is derived when increasing the **mPhTc$_2$** concentration to 3.5×10^{-4} M. Finally, at a concentration of 4.5×10^{-4}, I_{th} for **mPhTc$_2$** is, in fact, too low to be experimentally observed.

Finally, we unraveled respective contributions from intra-TTA-UC and intermolecular TTA-UC (inter-TTA-UC). The incident photon power densities were kept constant at 70.0 W/cm^{-2}, and the integrated fluorescence was calculated at variable concentrations of the dimeric acene annihilator in the presence of a constant concentration of **PdPc** (4×10^{-5} M, Figure 6b). Quantitatively, the integrated up-converted fluorescence is higher for the dimers than for the monomers across the entire concentration range. Overall, **mPhTc$_2$** gives rise to the highest integrated up-converted fluorescence. Strikingly, the up-converted fluorescence of **mPhTc$_2$** is detectable at concentrations as low as 1×10^{-6} M, where for the other tetracene derivatives no up-converted fluorescence was discernable.

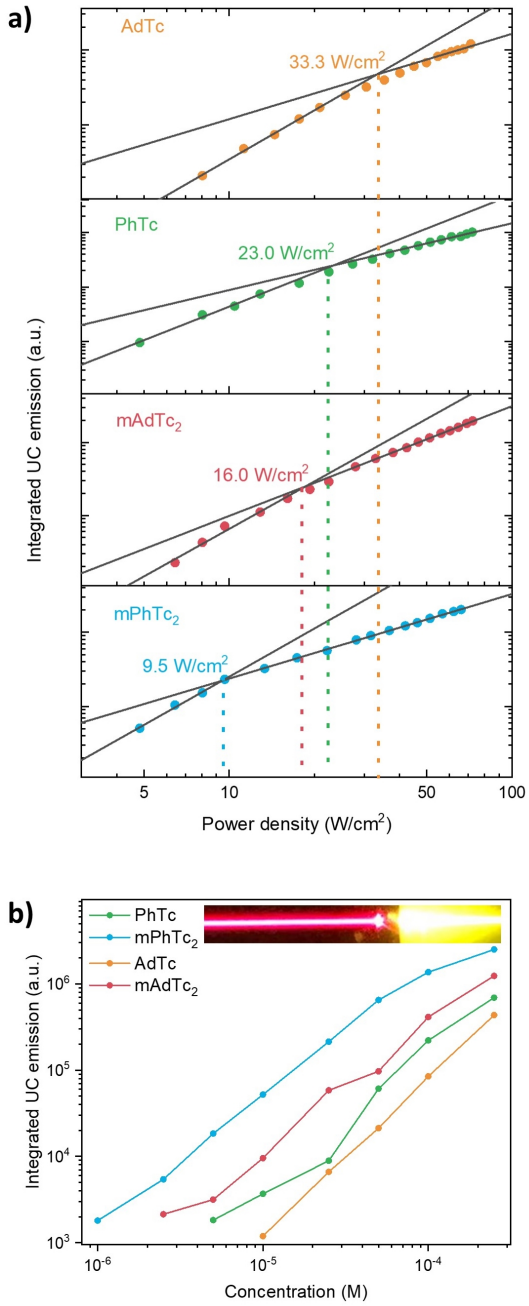

Figure 6. a) Power density dependence of the integrated up-converted emission of **AdTc, PhTc, mAdTc2,** and **mPhTc2**(2.5 × 10^{-4} M) with **PdPc** (4 × 10^{-5} M) in toluene; dashed lines show the power density thresholds. b): Log-log plots of integrated up-converted fluorescence as a function of the varied concentration of annihilators at a constant concentration of **PdPc** (4 × 10^{-5} M). Inset: Picture of the up-converted **mPhTc2** fluorescence via photoexcitation of **PdPc** at 730 nm.

To derive subtle details of TTA-UC, we determined the relative TTA-UC fluorescence quantum yields using a **TIPSTc/PdPc** system as a standard ($\Phi_{UC\text{-}F,std}$) (**TIPSTc** = 5,12-bis((triisopropylsilyl)ethynyl)tetracene, supporting information and Table 2). At annihilator concentrations as low as 1.0 × 10^{-5} M, where diffusion-controlled inter-TTA-UC is limited, $\Phi_{UC\text{-}F}$ is about 14 times larger for **mPhTc2** (0.031%) than for **PhTc** (0.0021%). Considering, however, that Φ_F for **mPhTc2** is much lower than for **PhTc** (Table 2), a 14-fold increase can only be rationalized through intra-TTA-UC contributions, which dominate over inter-TTA-UC contributions. Interestingly, $\Phi_{UC\text{-}F}$ of **mAdTc2** (0.0086%) at the same concentration is only around 9 times higher than that of **AdTc** (0.0010%). As such, intra-TTA-UC is more effective in **mPhTc2** than in **mAdTc2**. Stronger inter-tetracene electronic coupling in **mPhTc2**, which stems from the π-conjugated spacer, lowers the energy of $^1(T_1T_1)$ relative to that of $^{3/5}(T_1T_1)$. [81,82,83] Thus, formation of $^1(T_1T_1)$ is preferred and goes hand-in-hand with a larger spin statistical factor *f* and, therefore, higher $\Phi_{UC\text{-}F}$ for **mPhTc2**. Turning to higher concentrations of the annihilator (2.5 × 10^{-4} M), the differences in $\Phi_{UC\text{-}F}$ between the dimers and the corresponding monomers are rather subtle with $\Phi_{UC\text{-}F}$-ratios of around 3 for both pairs, **mPhTc2** (1.611%) and **PhTc** (0.444%) as well as **mAdTc2** (0.992%) and **AdTc** (0.345%). Two conclusions should be drawn at this stage. First, at high concentrations the dominance of intra-TTA-UC is lost as inter-TTA-UC becomes increasingly significant. Second, the nature of the spacer becomes less important at a point in which inter-TTA-UC contributions to the overall $\Phi_{UC\text{-}F}$ are significant. Overall, the superior TTA-UC performance of **mPhTc2** in the high concentration regime likely results from the synergy between inter- and intra-TTA.

Intramolecular Up-conversion We further elaborate on intra-TTA-UC in **mPhTc2** and **mAdTc2** by performing steady-state and time-resolved fluorescence spectroscopy under direct excitation at 480 nm. For both dimers, the absence of O_2 leads to an increase in fluorescence intensity especially for **mPhTc2** in toluene (Figure S34). This effect is less pronounced in the monomers. To be precise, Φ_F values for both dimers increase to ca. 30% in toluene and benzonitrile in the absence of O_2 (Table S4). Among both dimers, fluorescence for **mPhTc2** in toluene is the most sensitive to O_2, as Φ_F increases significantly by a factor of 4 compared to a factor of 2 for **mAdTc2** in toluene. Therefore, we conclude that intramolecular rather than intermolecular interactions, namely intra-TTA-UC, must be operative in the excited state decay of the dimers.

In time-correlated single photon counting (TCSPC) experiments, emission from **PhTc** and **AdTc** decays mono-exponentially with a lifetime of 10 ns that is independent of solvent polarity in a deoxygenated environment (Figures S38–S40; Tables S6 and 2). In contrast, the emission of **mPhTc2** and **mAdTc2** decays tri-exponentially and lasts for several hundreds of nanoseconds. It features one short and prompt (ps) as well as two long and delayed (ns) components. In toluene, **mPhTc2** shows lifetimes of <200 ps, 9.0 ns, and 58.7 ns with relative amplitudes of 3.2, 9.6, and 87.3%, respectively. For **mAdTc2**, the three lifetimes are 810 ps, 11.6 ns, and 59.1 ns and the relative amplitudes are 37.2, 49.5, and 13.3%. The agreement between the lifetimes from TCSPC and those from TAS measurements is solid (*vide supra*), for example, $(S_1S_0)_{rel}$ (80.0 ps), $(S_1S_0)_{(T1T1)^{CT}}$ (8.7 ns), and (T_1T_1) (66.5 ns) for mPhTc2 in toluene in TAS. Notably, the presence of O_2 accelerates the deactivation of all compounds and eliminates the emission from the longest-lived component for the dimers.

O_2-Sensitive fluorescence underpins the involvement of a triplet excited state during the radiative decay. In light of the fact that **mPhTc$_2$** and **mAdTc$_2$** undergo intra-SF, we posit that (T_1T_1) is involved in the delayed fluorescence. Two different scenarios are considered. On one hand, (T_1T_1) undergoes a direct radiative decay to the electronic ground state (S_0S_0), giving implicit spectral changes in the fluorescence spectrum.[43,84] On the other hand, since $E(S_1) \leq 2\times E(T_1)$ for tetracene, delayed fluorescence might also originate from $(S_1S_0)_{rel}$, which has been repopulated via TTA-UC. In that case no spectral changes are, however, expected over time. To clarify the nature of the delayed fluorescence, time-resolved emission spectroscopy (TRES) is recorded upon photoexcitation at 480 nm in the absence of O_2 (Figures 7 and S41–S43). In line with the TCSPC assays, **mPhTc$_2$** and **mAdTc$_2$** fluoresce well beyond hundreds of nanoseconds and without any discernable spectral changes through the entire timescale. Deconvolution of the TRES raw data by means of a three-species sequential kinetic model yields three spectroscopically identical fluorescence spectra. For example, fluorescence of **mPhTc$_2$** and **mAdTc$_2$** in toluene show maxima at 550 and 535 nm, respectively, throughout the entire deactivation process. This is in agreement with the corresponding steady-state fluorescence spectra.

In short, all three fluorescent components originate from the same state, namely $(S_1S_0)_{rel}$, and corroborate intra-TTA-UC in **mPhTc$_2$** and **mAdTc$_2$**. Thus, following direct photoexcitation, the prompt fluorescence comes directly from $(S_1S_0)_{rel}$ while the two delayed fluorescence events result from intramolecular up-converted fluorescence involving $(S_1S_0)_{(T1T1)}{}^{CT}$ and (T_1T_1). The relative amplitudes obtained from TCSPC for the emission resulting from up-converted (T_1T_1) are 87.3% for **mPhTc$_2$** and 13.3% for **mAdTc$_2$** in deoxygenated toluene, confirming that **mPhTc$_2$** is more efficient for intramolecular up-conversion due to stronger electronic coupling (Figure S40). Combining our results from steady-state and time-resolved absorption and emission spectroscopy we summarize the deactivation process of the dimers as illustrated in Figure 8.

Table 2. Lifetimes (τ) and relative amplitudes obtained from TCSPC of **AdTc**, **PhTc**, **mAdTc$_2$**, and **mPhTc$_2$** in O_2-free toluene, as well as up-conversion fluorescence quantum yields (Φ_{UC-F}) using a constant concentration of the **PdPc** sensitizer (4×10^{-5} M) and two different concentrations of the **AdTc**, **PhTc**, **mAdTc$_2$**, and **mPhTc$_2$** annihilators (2.5×10^{-4} and 1.0×10^{-5} M) in O_2-free toluene.

	TCSPC			Φ_{UC-F} [a] (%)	
	τ_1	τ_2	τ_3	2.5×10^{-4} (M)	1.0×10^{-5} (M)
PhTc	9.8 (100%)	-	-	0.444±0.074	0.0021±0.0003
mPhTc$_2$	< 200 ps [b] (3.16%)	9.0 (9.58%)	58.7 (87.26%)	1.611±0.225	0.0307±0.0031
$\frac{\Phi_{UC-F,\mathbf{mPhTc2}}}{\Phi_{UC-F,\mathbf{PhTc}}}$	-	-	-	3.6	14.6
AdTc	12.5 (100%)	-	-	0.345±0.075	0.0010±0.0003
mAdTc$_2$	810 ps (37.17%)	11.6 (49.51%)	59.1 (13.32%)	0.992±0.222	0.0086±0.0025
$\frac{\Phi_{UC-F,\mathbf{mAdTc2}}}{\Phi_{UC-F,\mathbf{AdTc}}}$	-	-	-	2.9	8.6

[a] Average values of Φ_{UC-F} and standard deviations are obtained from three different measurements.
[b] The lifetime is below the resolution limit of our TCSPC setup.

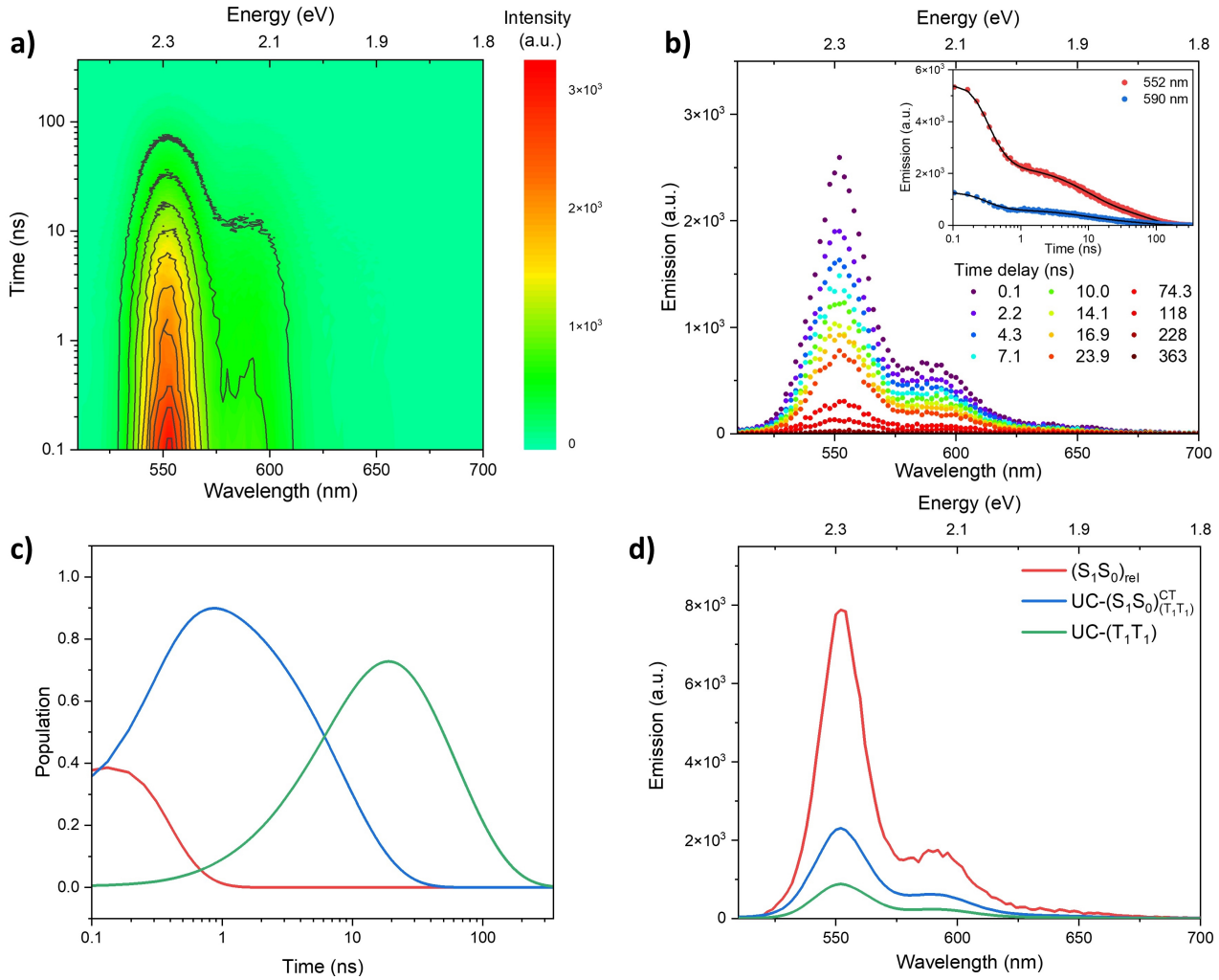

Figure 7. Global Analysis of the TRES raw data for **mPhTc₂** following photoexcitation at 480 nm in argon-saturated toluene at room temperature. a) Heat map of TRES raw data. b) Emission spectra at various time delays. Insert: Time absorption profiles as well as corresponding fits of selected wavelengths (see the figure legend for details). c) Relative populations of the respective species with colors correlating with the evolution associated spectra (EAS). d) EAS of the deconvoluted species: the first species is the fluorescent relaxed singlet excited state $(S_1S_0)_{rel}$ (red), the second species is the up-converted fluorescent $(S_1S_0)_{rel}$ from the intermediate state $(S_1S_0)_{(T1T1)}{}^{CT}$ (blue), and the third species is the up-converted fluorescent $(S_1S_0)_{rel}$ from the correlated triplet pair (T_1T_1) (green).

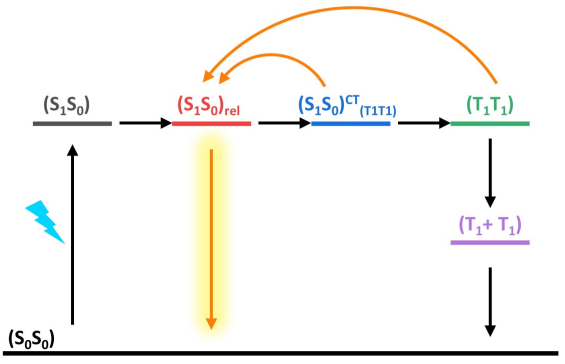

Figure 8. Schematic representations of intra-SF (black arrows) and intra-TTA-UC (orange arrows) after 480 nm photoexcitation of **mPhTc2** and **mAdTc2** in argon-saturated toluene and benzonitrile. The relaxed singlet excited state $(S_1S_0)_{rel}$ is the sole fluorescent state, and its radiative deactivation is highlighted in yellow. The species are marked by the same colors as the corresponding spectra in TAS and TRES with the singlet excited state (S_1S_0) in grey, the relaxed singlet excited state $(S_1S_0)_{rel}$ in red, the intermediate state $(S_1S_0)_{(T1T1)}{}^{CT}$ in blue, the correlated triplet pair (T_1T_1) in green, and the state representing uncorrelated triplet excited states $(T_1 + T_1)$ in violet.

Thermal Effects in Down- and Up-Conversion To better document the interplay between intra-SF and intra-TTA-UC, we studied thermal effects in **mPhTc₂** and **mAdTc₂** under direct photoexcitation by means of temperature-dependent steady-state absorption and emission spectroscopy, TCSPC, as well as fs- and ns-TAS. For this purpose, we varied the temperature stepwise from 300 to 80 K. To start, we inspected the thermal effects on the

steady-state absorption spectra in O_2-free 2-methyl-tetrahydrofuran (MeTHF), as shown in Figures S44a and S45a. As the temperature is lowered, the absorptions of both dimers undergo a slight bathochromic shift and feature increased oscillator strengths in addition to sharper vibrational structure. Overall, the shape of the spectra is, however, temperature-independent. At the same time, the fluorescence of both dimers sharpens and shifts bathochromically while maintaining the same overall profile (Figures S44b and S45b). Strikingly, the fluorescence intensity of **mAdTc$_2$** increases dramatically with decreasing temperature. To factor out increasing oscillator strength in the absorption spectra upon lowering the temperature, we calibrated the integrated fluorescence by means of dividing it by the optical density at the photoexcitation wavelength. The calibrated integrated fluorescence of **mPhTc$_2$** remains constant as a function of temperature, indicating temperature-independent fluorescence quantum yields of **mPhTc$_2$** (Figure S44b insert). In contrast, the calibrated integrated fluorescence of **mAdTc$_2$** increases as the temperature is decreased. In particular, the calibrated integrated fluorescence at 80 K is around 3 times greater than at 300 K (Figure S45b insert). Therefore, radiative deactivation of **mAdTc$_2$** is more likely to occur at low temperature.

Next, we turned to thermal effects on the radiative deactivation pathways using temperature-dependent TCSPC in O_2-free MeTHF (Figures S46 and S47 and Table S7). For **mPhTc$_2$**, the prompt $(S_1S_0)_{rel}$ lifetime is below the instrumental time resolution. The lifetime of the second component, that is $(S_1S_0)_{(T1T1)}{}^{CT}$, displays little temperature dependence. The remaining long lifetime, namely that of (T_1T_1), increases from 50.2 ns at 300 K to 148.0 ns at 80 K with relative amplitudes of 68.5 and 18.8%, respectively. Hence, TTA-UC from (T_1T_1) contributes less to the overall emission at lower temperatures. Our observations indicate that TTA-UC from (T_1T_1) is thermally activated for **mPhTc$_2$**. According to the Arrhenius plot (Figure S48), the activation barrier for intra-TTA-UC in **mPhTc$_2$** is around 0.011 ± 0.003 eV.[85] Turning to **mAdTc$_2$**, the lifetime of $(S_1S_0)_{rel}$ increases from 0.7 ns at 300 K to 3.0 ns at 80 K. Temperature dependence is not noted for the lifetime of $(S_1S_0)_{(T1T1)}{}^{CT}$, while that of (T_1T_1) becomes longer as the temperature is reduced. As a matter of fact, intra-TTA-UC from (T_1T_1) is shut down completely below 160 K, as a biexponential fitting turned out to be sufficient for the TCSPC data. For **mAdTc$_2$**, the activation barrier by means of Arrhenius analysis is around 0.03 eV.[86] Higher fluorescence quantum yields of **mAdTc$_2$** at lower temperatures relate to a radiative decay even before (T_1T_1) is formed.

In the final part of our analysis, thermal effects on intra-SF have been investigated by means of temperature-dependent fs- and ns-TAS in O_2-free MeTHF. The raw data is fitted according to the sequential kinetic model shown in Figure S32.[87] As Figures S49-52and Tables S8 and S9 illustrate, we detect all key steps of intra-SF across the temperature range from 80 to 300 K, for both dimers. The lifetimes of $(S_1S_0)_{rel}$, $(S_1S_0)_{(T1T1)}{}^{CT}$, and (T_1T_1) are in sound agreement with the TCSPC results. Notably, the lifetime of $(S_1S_0)_{rel}$ for **mPhTc$_2$** is temperature independent with a constant value of ca. 100 ps (Table S11). For **mAdTc$_2$**, however, the lifetime of $(S_1S_0)_{rel}$ increases from ca. 800 ps at 300 K to ca. 2.4 ns at temperatures below 120 K. We assume that the formation of the superposition of $(S_1S_0)_{rel}$, the CT state, and $^1(T_1T_1)$ requires vibronic coupling of the involved states. The restricted motion of the nuclei at lower temperatures, therefore, slows the generation of the superposition, namely the formation of $(S_1S_0)_{(T1T1)}{}^{CT}$. For **mPhTc$_2$**, however, the stronger electronic coupling reduces the extent of nuclei motion required to generate $(S_1S_0)_{(T1T1)}{}^{CT}$. Consequently, the formation of $(S_1S_0)_{(T1T1)}{}^{CT}$ in **mPhTc$_2$** is less sensitive to temperature. Subsequently, $(S_1S_0)_{(T1T1)}{}^{CT}$ exhibits constant lifetimes of 8–10 ns upon cooling in both dimers. We attribute this to the fact that the dephasing is driven mainly by electronic processes and requires less nuclei motion. Overall, intra-SF for **mAdTc$_2$** is temperature dependent, while for **mPhTc2** it is temperature independent. To further elaborate on this, we have determined the relative triplet quantum yields ($\Phi_{r\text{-}T}$)[88] of **mPhTc$_2$** and **mAdTc$_2$** by comparing the GSB intensities of the EAS of $(S_1S_0)_{(T1T1)}{}^{CT}$ and (T_1T_1) (Table S12). Upon cooling from 300 to 80 K, $\Phi_{r\text{-}T}$ of **mPhTc$_2$** remains constant at ca. 70–80%. For **mAdTc$_2$**, a decrease in temperature reduces $\Phi_{r\text{-}T}$ from 84% at 300 K to 32% at 80 K, indicating that intra-SF is less efficient at lower temperatures. This finding is in sound agreement with our results from temperature-dependent steady-state and time-resolved emission measurements, namely enhanced radiative deactivation accompanied by the loss of the up-converted emission from (T_1T_1) of **mAdTc$_2$** at low temperatures.

Conclusion

We have explored two tetracene dimers that feature either a 1,3-diethynyladamantyl (**mAdTc$_2$**) or a phenylene spacer (**mPhTc$_2$**) and that are designed to fine-tune the intramolecular coupling between the tetracene chromophores while conserving an identical spatial relationship. Down- and up-conversion have been characterized, especially in comparison with the corresponding monomers **PhTc** and **AdTc**. Following photoexcitation, intra-SF operates efficiently in both dimers, with over 100% triplet quantum yields, and is mediated by a superposition of (S_1S_0), a CT state, and $^1(T_1T_1)$. In photosensitized up-conversion measurements with the assistance of **PdPc**, intra-TTA-UC is confirmed in both dimers. The dimer **mPhTc$_2$** exhibits a better up-conversion performance due to more efficient intra-TTA that results from stronger inter-tetracene coupling. Independent evidence for intra-TTA-UC comes from direct excitation of the tetracene dimers, which leads to delayed up-converted fluorescence from the intermediate state $(S_1S_0)_{(T1T1)}{}^{CT}$ and the correlated triplet pair (T_1T_1) alongside prompt $(S_1S_0)_{rel}$ fluorescence. Inter-tetracene coupling is the decisive factor that governs the fate of (T_1T_1). On one hand, the more strongly coupled, π-cross-conjugated phenylene-linked **mPhTc$_2$** favors TTA-UC from (T_1T_1). On the other hand, the more weakly coupled, non-conjugated 1,3-diethynyladamantyl spacer of **mAdTc$_2$** supports efficient (T_1T_1) decorrelation, which is vital for efficient intra-SF. To round off the studies on the interplay between intra-SF and intra-TTA-UC, temperature-dependent measurements have been carried out under direct

photoexcitation of the dimers. At low temperatures, intra-SF of **mAdTc$_2$** is slowed down significantly and consequently, no intra-TTA-UC is observed. However, both intra-TTA-UC and intra-SF of **mPhTc$_2$** are active even at 80 K due to stronger electronic coupling between the two tetracene chromophores. The current work defines our understanding of the potentially competitive processes of down- and up-conversion, providing design principles for chromophores that lead to either efficient TTA-UC or the generation of uncorrelated triplet excited states formed via intra-SF.

ASSOCIATED CONTENT

Supporting Information.

AUTHOR INFORMATION

Corresponding Author

* dirk.guldi@fau.de
* rik.tykwinski@ualberta.ca

ORCID

Yifan Bo: orcid.org/ 0000-0002-4531-4789
Yuxuan Hou: orcid.org/ 0000-0002-5783-9590
Dominik Thiel: orcid.org/0000-0002-3427-2042
René Weiß: orcid.org/0000-0002-7278-8111
Timothy Clark: orcid.org/0000-0001-7931-4659
Michael J. Ferguson: orcid.org/0000-0002-5221-4401
Rik R. Tykwinski: orcid.org/0000-0002-7645-4784
Dirk M. Guldi: orcid.org/0000-0002-3960-1765

Notes

The authors declare no competing financial interest.

ACKNOWLEDGMENT

We are grateful for funding from the Natural Sciences and Engineering Research Council of Canada (NSERC) and Canada Foundation for Innovation (CFI). We thank the National Renewable Energy Laboratory (NREL) for the solar spectra in the table of contents figure.

REFERENCES

(1) Hansen, J.; Kharecha, P.; Sato, M.; Masson-Delmotte, V.; Ackerman, F.; Beerling, D. J.; Hearty, P. J.; Hoegh-Guldberg, O.; Hsu, S. L.; Parmesan, C.; Rockstrom, J.; Rohling, E. J.; Sachs, J.; Smith, P.; Steffen, K.; Van Susteren, L.; Von Schuckmann, K.; Zachos, J. C. Assessing "Dangerous Climate Change": Required Reduction of Carbon Emissions to Protect Young People, Future Generations and Nature. *PLoS One* **2013**, *8* (12), e81648. https://doi.org/10.1371/journal.pone.0081648.

(2) Blankenship, R. E.; Tiede, D. M.; Barber, J.; Brudvig, G. W.; Fleming, G.; Ghirardi, M.; Gunner, M. R.; Junge, W.; Kramer, D. M.; Melis, A.; Moore, T. A.; Moser, C. C.; Nocera, D. G.; Nozik, A. J.; Ort, D. R.; Parson, W. W.; Prince, R. C.; Sayre, R. T. Comparing Photosynthetic and Photovoltaic Efficiencies and Recognizing the Potential for Improvement. *Science* **2011**, *332* (6031), 805–809. https://doi.org/10.1126/science.1200165.

(3) Hirst, L. C.; Ekins-Daukes, N. J. Quantifying Intrinsic Loss Mechanisms in Solar Cells: Why Is Power Efficiency Fundamentally Limited? *Next Gener. Photonic Cell Technol. Sol. Energy Convers.* **2010**, *7772* (May), 777211. https://doi.org/10.1117/12.860681.

(4) Shockley, W.; Queisser, H. J. Detailed Balance Limit of Efficiency of P-n Junction Solar Cells. *J. Appl. Phys.* **1961**, *32* (3), 510–519. https://doi.org/10.1063/1.1736034.

(5) Beery, D.; Schmidt, T. W.; Hanson, K. Harnessing Sunlight via Molecular Photon Upconversion. *ACS Appl. Mater. Interfaces* **2021**, *13* (28), 32601–32605. https://doi.org/10.1021/acsami.1c08159.

(6) Rao, A.; Friend, R. H. Harnessing Singlet Exciton Fission to Break the Shockley–Queisser Limit. *Nat. Rev. Mater.* **2017**, *2* (11), 17063. https://doi.org/10.1038/natrevmats.2017.63.

(7) Efficiency, C. *Emerging Strategies to Reduce Transmission and Thermalization Losses in Solar Cells*; 2022. https://doi.org/10.1007/978-3-030-70358-5.

(8) Xia, J.; Sanders, S. N.; Cheng, W.; Low, J. Z.; Liu, J.; Campos, L. M.; Sun, T. Singlet Fission: Progress and Prospects in Solar Cells. *Adv. Mater.* **2017**, *29* (20), 1601652. https://doi.org/10.1002/adma.201601652.

(9) Smith, M. B.; Michl, J. Recent Advances in Singlet Fission. *Annu. Rev. Phys. Chem.* **2013**, *64* (1), 361–386. https://doi.org/10.1146/annurev-physchem-040412-110130.

(10) Gholizadeh, E. M.; Prasad, S. K. K.; Teh, Z. L.; Ishwara, T.; Norman, S.; Petty, A. J.; Cole, J. H.; Cheong, S.; Tilley, R. D.; Anthony, J. E.; Huang, S.; Schmidt, T. W. Photochemical Upconversion of Near-Infrared Light from below the Silicon Bandgap. *Nat. Photonics* **2020**, *14* (9), 585–590. https://doi.org/10.1038/s41566-020-0664-3.

(11) Casillas, R.; Papadopoulos, I.; Ullrich, T.; Thiel, D.; Kunzmann, A.; Guldi, D. M. Molecular Insights and Concepts to Engineer Singlet Fission Energy Conversion Devices. *Energy Environ. Sci.* **2020**, *13* (9), 2741–2804. https://doi.org/10.1039/d0ee00495b.

(12) Smith, M. B.; Michl, J. Singlet Fission. *Chem. Rev.* **2010**, *110* (11), 6891–6936. https://doi.org/10.1021/cr1002613.

(13) Ullrich, T.; Munz, D.; Guldi, D. M. Unconventional Singlet Fission Materials. *Chem. Soc. Rev.* **2021**, *50* (5), 3485–3518. https://doi.org/10.1039/d0cs01433h.

(14) Burdett, J. J.; Bardeen, C. J. Quantum Beats in Crystalline Tetracene Delayed Fluorescence Due to Triplet Pair Coherences Produced by Direct Singlet Fission. *J. Am. Chem. Soc.* **2012**, *134* (20), 8597–8607. https://doi.org/10.1021/ja301683w.

(15) Fuemmeler, E. G.; Sanders, S. N.; Pun, A. B.; Kumarasamy, E.; Zeng, T.; Miyata, K.; Steigerwald, M. L.; Zhu, X. Y.; Sfeir, M. Y.; Campos, L. M.; Ananth, N. A Direct Mechanism of Ultrafast Intramolecular Singlet Fission in Pentacene Dimers. *ACS Cent. Sci.* **2016**, *2* (5), 316–324. https://doi.org/10.1021/acscentsci.6b00063.

(16) Zimmerman, P. M.; Musgrave, C. B.; Head-Gordon, M. A Correlated Electron View of Singlet Fission. *Acc. Chem. Res.* **2013**, *46* (6), 1339–1347. https://doi.org/10.1021/ar3001734.

(17) Papadopoulos, I.; Zirzlmeier, J.; Hetzer, C.; Bae, Y. J.; Krzyaniak, M. D.; Wasielewski, M. R.; Clark, T.; Tykwinski, R. R.; Guldi, D. M. Varying the Interpentacene Electronic Coupling to Tune Singlet Fission. *J. Am. Chem. Soc.* **2019**, *141* (15), 6191–6203. https://doi.org/10.1021/jacs.8b09510.

(18) Basel, B. S.; Zirzlmeier, J.; Hetzer, C.; Reddy, S. R.; Phelan, B. T.; Krzyaniak, M. D.; Volland, M. K.; Coto, P. B.; Young, R. M.; Clark, T.; Thoss, M.; Tykwinski, R. R.; Wasielewski, M. R.; Guldi, D. M. Evidence for Charge-Transfer Mediation in the Primary Events of Singlet Fission in a Weakly Coupled Pentacene Dimer. *Chem* **2018**, *4* (5), 1092–1111. https://doi.org/10.1016/j.chempr.2018.04.006.

(19) Berkelbach, T. C.; Hybertsen, M. S.; Reichman, D. R. Microscopic Theory of Singlet Exciton Fission. I. General Formulation. *J. Chem. Phys.* **2013**, *138* (11). https://doi.org/10.1063/1.4794425.

(20) Monahan, N.; Zhu, X.-Y. Charge Transfer–Mediated Singlet Fission. *Annu. Rev. Phys. Chem.* **2015**, *66* (1), 601–618. https://doi.org/10.1146/annurev-physchem-040214-

121235.
(21) Lukman, S.; Chen, K.; Hodgkiss, J. M.; Turban, D. H. P.; Hine, N. D. M.; Dong, S.; Wu, J.; Greenham, N. C.; Musser, A. J. Tuning the Role of Charge-Transfer States in Intramolecular Singlet Exciton Fission through Side-Group Engineering. *Nat. Commun.* **2016**, *7*, 1–13. https://doi.org/10.1038/ncomms13622.
(22) Margulies, E. A.; Miller, C. E.; Wu, Y.; Ma, L.; Schatz, G. C.; Young, R. M.; Wasielewski, M. R. Enabling Singlet Fission by Controlling Intramolecular Charge Transfer in π-Stacked Covalent Terrylenediimide Dimers. *Nat. Chem.* **2016**, *8* (12), 1120–1125. https://doi.org/10.1038/nchem.2589.
(23) Papadopoulos, I.; Álvaro-Martins, M. J.; Molina, D.; McCosker, P. M.; Keller, P. A.; Clark, T.; Sastre-Santos, Á.; Guldi, D. M. Solvent-Dependent Singlet Fission in Diketopyrrolopyrrole Dimers: A Mediating Charge Transfer versus a Trapping Symmetry-Breaking Charge Separation. *Adv. Energy Mater.* **2020**, *10* (43), 2001496. https://doi.org/10.1002/aenm.202001496.
(24) Young, R. M.; Wasielewski, M. R. Mixed Electronic States in Molecular Dimers: Connecting Singlet Fission, Excimer Formation, and Symmetry-Breaking Charge Transfer. *Acc. Chem. Res.* **2020**, *53* (9), 1957–1968. https://doi.org/10.1021/acs.accounts.0c00397.
(25) Kim, W.; Musser, A. J. Tracking Ultrafast Reactions in Organic Materials through Vibrational Coherence: Vibronic Coupling Mechanisms in Singlet Fission. *Adv. Phys. X* **2021**, *6* (1). https://doi.org/10.1080/23746149.2021.1918022.
(26) Chan, W. L.; Berkelbach, T. C.; Provorse, M. R.; Monahan, N. R.; Tritsch, J. R.; Hybertsen, M. S.; Reichman, D. R.; Gao, J.; Zhu, X. Y. The Quantum Coherent Mechanism for Singlet Fission: Experiment and Theory. *Acc. Chem. Res.* **2013**, *46* (6), 1321–1329. https://doi.org/10.1021/ar300286s.
(27) Zhao, X.; O'Connor, J. P.; Schultz, J. D.; Bae, Y. J.; Lin, C.; Young, R. M.; Wasielewski, M. R. Temperature Tuning of Coherent Mixing between States Driving Singlet Fission in a Spiro-Fused Terrylenediimide Dimer. *J. Phys. Chem. B* **2021**, *125* (25), 6945–6954. https://doi.org/10.1021/acs.jpcb.1c02476.
(28) Mandal, A.; Chen, M.; Foszcz, E. D.; Schultz, J. D.; Kearns, N. M.; Young, R. M.; Zanni, M. T.; Wasielewski, M. R. Two-Dimensional Electronic Spectroscopy Reveals Excitation Energy-Dependent State Mixing during Singlet Fission in a Terrylenediimide Dimer. *J. Am. Chem. Soc.* **2018**, *140* (51), 17907–17914. https://doi.org/10.1021/jacs.8b08627.
(29) Chen, M.; Bae, Y. J.; Mauck, C. M.; Mandal, A.; Young, R. M.; Wasielewski, M. R. Singlet Fission in Covalent Terrylenediimide Dimers: Probing the Nature of the Multiexciton State Using Femtosecond Mid-Infrared Spectroscopy. *J. Am. Chem. Soc.* **2018**, *140* (29), 9184–9192. https://doi.org/10.1021/jacs.8b04830.
(30) Gotfredsen, H.; Thiel, D.; Greißel, P. M.; Chen, L.; Krug, M.; Papadopoulos, I.; Ferguson, M. J.; Nielsen, M. B.; Clark, T.; Guldi, D. M.; Tykwinski, R. R.; Torres, T.; Clark, T.; Guldi, D. M.; Tykwinski, R. R. Sensitized Singlet Fission in Rigidly Linked Axial and Peripheral Pentacene-Subphthalocyanine Conjugates. *J. Am. Chem. Soc.* **2022**, *1*. https://doi.org/10.1021/jacs.2c13353.
(31) Miyata, K.; Conrad-Burton, F. S.; Geyer, F. L.; Zhu, X. Y. Triplet Pair States in Singlet Fission. *Chem. Rev.* **2019**, *119* (6), 4261–4292. https://doi.org/10.1021/acs.chemrev.8b00572.
(32) Xu, R.; Zhang, C.; Xiao, M. Magnetic Field Effects on Singlet Fission Dynamics. *Trends Chem.* **2022**, *4* (6), 528–539. https://doi.org/10.1016/j.trechm.2022.03.009.
(33) Musser, A. J.; Clark, J. Triplet-Pair States in Organic Semiconductors. *Annu. Rev. Phys. Chem.* **2019**, *70* (1), 323–351. https://doi.org/10.1146/annurev-physchem-042018-052435.
(34) Basel, B. S.; Zirzlmeier, J.; Hetzer, C.; Phelan, B. T.; Krzyaniak, M. D.; Reddy, S. R.; Coto, P. B.; Horwitz, N. E.; Young, R. M.; White, F. J.; Hampel, F.; Clark, T.; Thoss, M.; Tykwinski, R. R.; Wasielewski, M. R.; Guldi, D. M. Unified Model for Singlet Fission within a Non-Conjugated Covalent Pentacene Dimer. *Nat. Commun.* **2017**, *8* (May), 1–8. https://doi.org/10.1038/ncomms15171.
(35) Chen, M.; Krzyaniak, M. D.; Nelson, J. N.; Bae, Y. J.; Harvey, S. M.; Schaller, R. D.; Young, R. M.; Wasielewski, M. R. Quintet-Triplet Mixing Determines the Fate of the Multiexciton State Produced by Singlet Fission in a Terrylenediimide Dimer at Room Temperature. *Proc. Natl. Acad. Sci. U. S. A.* **2019**, *116* (17), 8178–8183. https://doi.org/10.1073/pnas.1820932116.
(36) Weiss, L. R.; Bayliss, S. L.; Kraffert, F.; Thorley, K. J.; Anthony, J. E.; Bittl, R.; Friend, R. H.; Rao, A.; Greenham, N. C.; Behrends, J. Strongly Exchange-Coupled Triplet Pairs in an Organic Semiconductor. *Nat. Phys.* **2017**, *13* (2), 176–181. https://doi.org/10.1038/nphys3908.
(37) Tayebjee, M. J. Y.; Sanders, S. N.; Kumarasamy, E.; Campos, L. M.; Sfeir, M. Y.; McCamey, D. R. Quintet Multiexciton Dynamics in Singlet Fission. *Nat. Phys.* **2017**, *13* (2), 182–188. https://doi.org/10.1038/nphys3909.
(38) Casanova, D. Theoretical Modeling of Singlet Fission. *Chem. Rev.* **2018**, *118* (15), 7164–7207. https://doi.org/10.1021/acs.chemrev.7b00601.
(39) Kolomeisky, A. B.; Feng, X.; Krylov, A. I. A Simple Kinetic Model for Singlet Fission: A Role of Electronic and Entropic Contributions to Macroscopic Rates. *J. Phys. Chem. C* **2014**, *118* (10), 5188–5195. https://doi.org/10.1021/jp4128176.
(40) Hetzer, C.; Basel, B. S.; Kopp, S. M.; Hampel, F.; White, F. J.; Clark, T.; Guldi, D. M.; Tykwinski, R. R. Chromophore Multiplication To Enable Exciton Delocalization and Triplet Diffusion Following Singlet Fission in Tetrameric Pentacene. *Angew. Chemie Int. Ed.* **2019**, 1–6. https://doi.org/10.1002/anie.201907221.
(41) Basel, B. S.; Hetzer, C.; Zirzlmeier, J.; Thiel, D.; Guldi, R.; Hampel, F.; Kahnt, A.; Clark, T.; Guldi, D. M.; Tykwinski, R. R. Davydov Splitting and Singlet Fission in Excitonically Coupled Pentacene Dimers. *Chem. Sci.* **2019**, *10* (13), 3854–3863. https://doi.org/10.1039/c9sc00384c.
(42) Wilson, M. W. B.; Rao, A.; Johnson, K.; Gélinas, S.; Di Pietro, R.; Clark, J.; Friend, R. H. Temperature-Independent Singlet Exciton Fission in Tetracene. *J. Am. Chem. Soc.* **2013**, *135* (44), 16680–16688. https://doi.org/10.1021/ja408854u.
(43) Stern, H. L.; Cheminal, A.; Yost, S. R.; Broch, K.; Bayliss, S. L.; Chen, K.; Tabachnyk, M.; Thorley, K.; Greenham, N.; Hodgkiss, J. M.; Anthony, J.; Head-Gordon, M.; Musser, A. J.; Rao, A.; Friend, R. H. Vibronically Coherent Ultrafast Triplet-Pair Formation and Subsequent Thermally Activated Dissociation Control Efficient Endothermic Singlet Fission. *Nat. Chem.* **2017**, *9* (12), 1205–1212. https://doi.org/10.1038/nchem.2856.
(44) Burdett, J. J.; Müller, A. M.; Gosztola, D.; Bardeen, C. J. Excited State Dynamics in Solid and Monomeric Tetracene: The Roles of Superradiance and Exciton Fission. *J. Chem. Phys.* **2010**, *133* (14). https://doi.org/10.1063/1.3495764.
(45) Budden, P. J.; Weiss, L. R.; Müller, M.; Panjwani, N. A.; Dowland, S.; Allardice, J. R.; Ganschow, M.; Freudenberg, J.; Behrends, J.; Bunz, U. H. F.; Friend, R. H. Singlet Exciton Fission in a Modified Acene with Improved Stability and High Photoluminescence Yield. *Nat. Commun.* **2021**, *12* (1), 1–8. https://doi.org/10.1038/s41467-021-21719-x.
(46) Müller, A. M.; Avlasevich, Y. S.; Schoeller, W. W.; Müllen, K.; Bardeen, C. J. Exciton Fission and Fusion in Bis(Tetracene) Molecules with Different Covalent Linker Structures. *J. Am. Chem. Soc.* **2007**, *129* (46), 14240–14250. https://doi.org/10.1021/ja073173y.
(47) Matsui, Y.; Kawaoka, S.; Nagashima, H.; Nakagawa, T.; Okamura, N.; Ogaki, T.; Ohta, E.; Akimoto, S.; Sato-Tomita, A.; Yagi, S.; Kobori, Y.; Ikeda, H. Exergonic Intramolecular Singlet Fission of an Adamantane-Linked Tetracene Dyad via Twin Quintet Multiexcitons. *J. Phys. Chem. C* **2019**, *123* (31), 18813–18823. https://doi.org/10.1021/acs.jpcc.9b04503.
(48) Gao, C.; Wong, W. W. H. H.; Qin, Z.; Lo, S. C.; Namdas, E. B.; Dong, H.; Hu, W. Application of Triplet–Triplet Annihilation Upconversion in Organic Optoelectronic Devices: Advances and Perspectives. *Adv. Mater.* **2021**, *2100704* (45), 2100704.

https://doi.org/10.1002/adma.202100704.

(49) Bharmoria, P.; Bildirir, H.; Moth-Poulsen, K. Triplet-Triplet Annihilation Based near Infrared to Visible Molecular Photon Upconversion. *Chem. Soc. Rev.* **2020**, *49* (18), 6529–6554. https://doi.org/10.1039/d0cs00257g.

(50) Seo, S. E.; Choe, H.-S.; Cho, H.; Kim, H.; Kim, J.; Kwon, O. S. Recent Advances in Materials for and Applications of Triplet-Triplet Annihilation-Based Upconversion. *J. Mater. Chem. C* **2021**. https://doi.org/10.1039/d1tc03551g.

(51) Singh-Rachford, T. N.; Castellano, F. N. Photon Upconversion Based on Sensitized Triplet-Triplet Annihilation. *Coord. Chem. Rev.* **2010**, *254* (21–22), 2560–2573. https://doi.org/10.1016/j.ccr.2010.01.003.

(52) Ieuji, R.; Goushi, K.; Adachi, C. Triplet–Triplet Upconversion Enhanced by Spin–Orbit Coupling in Organic Light-Emitting Diodes. *Nat. Commun.* **2019**, *10* (1). https://doi.org/10.1038/s41467-019-13044-1.

(53) Sanders, S. N.; Schloemer, T. H.; Gangishetty, M. K.; Anderson, D.; Seitz, M.; Gallegos, A. O.; Stokes, R. C.; Congreve, D. N. Triplet Fusion Upconversion Nanocapsules for Volumetric 3D Printing. *Nature* **2022**, *604* (7906), 474–478. https://doi.org/10.1038/s41586-022-04485-8.

(54) Mattiello, S.; Mecca, S.; Ronchi, A.; Calascibetta, A.; Mattioli, G.; Pallini, F.; Meinardi, F.; Beverina, L.; Monguzzi, A. Diffusion-Free Intramolecular Triplet-Triplet Annihilation in Engineered Conjugated Chromophores for Sensitized Photon Upconversion. *ACS Energy Lett.* **2022**, *7* (8), 2435–2442. https://doi.org/10.1021/acsenergylett.2c01224.

(55) Imperiale, C. J.; Green, P. B.; Miller, E. G.; Damrauer, N. H.; Wilson, M. W. B. Triplet-Fusion Upconversion Using a Rigid Tetracene Homodimer. *J. Phys. Chem. Lett.* **2019**, *10* (23), 7463–7469. https://doi.org/10.1021/acs.jpclett.9b03115.

(56) Fallon, K. J.; Churchill, E. M.; Sanders, S. N.; Shee, J.; Weber, J. L.; Meir, R.; Jockusch, S.; Reichman, D. R.; Sfeir, M. Y.; Congreve, D. N.; Campos, L. M. Molecular Engineering of Chromophores to Enable Triplet-Triplet Annihilation Upconversion. *J. Am. Chem. Soc.* **2020**, *142* (47), 19917–19925. https://doi.org/10.1021/jacs.0c06386.

(57) Pun, A. B.; Sanders, S. N.; Sfeir, M. Y.; Campos, L. M.; Congreve, D. N. Annihilator Dimers Enhance Triplet Fusion Upconversion. *Chem. Sci.* **2019**, *10* (14), 3969–3975. https://doi.org/10.1039/C8SC03725F.

(58) Huang, L.; Le, T.; Huang, K.; Han, G. Enzymatic Enhancing of Triplet–Triplet Annihilation Upconversion by Breaking Oxygen Quenching for Background-Free Biological Sensing. *Nat. Commun.* **2021**, *12* (1), 1–9. https://doi.org/10.1038/s41467-021-22282-1.

(59) Felter, K. M.; Fravventura, M. C.; Koster, E.; Abellon, R. D.; Savenije, T. J.; Grozema, F. C. Solid-State Infrared Upconversion in Perylene Diimides Followed by Direct Electron Injection. *ACS Energy Lett.* **2020**, *5* (1), 124–129. https://doi.org/10.1021/acsenergylett.9b02361.

(60) Huang, L.; Wu, W.; Li, Y.; Huang, K.; Zeng, L.; Lin, W.; Han, G. Highly Effective Near-Infrared Activating Tripleta-Triplet Annihilation Upconversion for Photoredox Catalysis. *J. Am. Chem. Soc.* **2020**, *142* (43), 18460–18470. https://doi.org/10.1021/jacs.0c06976.

(61) Olesund, A.; Gray, V.; Mårtensson, J.; Albinsson, B. Diphenylanthracene Dimers for Triplet-Triplet Annihilation Photon Upconversion: Mechanistic Insights for Intramolecular Pathways and the Importance of Molecular Geometry. *J. Am. Chem. Soc.* **2021**, *143* (15), 5745–5754. https://doi.org/10.1021/jacs.1c00331.

(62) Sanders, S. N.; Kumarasamy, E.; Fallon, K. J.; Sfeir, M. Y.; Campos, L. M. Singlet Fission in a Hexacene Dimer: Energetics Dictate Dynamics. *Chem. Sci.* **2020**, *11* (4), 1079–1084. https://doi.org/10.1039/c9sc05066c.

(63) Korovina, N. V.; Das, S.; Nett, Z.; Feng, X.; Joy, J.; Haiges, R.; Krylov, A. I.; Bradforth, S. E.; Thompson, M. E. Singlet Fission in a Covalently Linked Cofacial Alkynyltetracene Dimer. *J. Am. Chem. Soc.* **2016**, *138* (2), 617–627. https://doi.org/10.1021/jacs.5b10550.

(64) Korovina, N. V.; Joy, J.; Feng, X.; Feltenberger, C.; Krylov, A. I.; Bradforth, S. E.; Thompson, M. E. Linker-Dependent Singlet Fission in Tetracene Dimers. *J. Am. Chem. Soc.* **2018**, *140* (32), 10179–10190. https://doi.org/10.1021/jacs.8b04401.

(65) Wang, Z.; Liu, H.; Xie, X.; Zhang, C.; Wang, R.; Chen, L.; Xu, Y.; Ma, H.; Fang, W.; Yao, Y.; Sang, H.; Wang, X.; Li, X.; Xiao, M. Free-Triplet Generation with Improved Efficiency in Tetracene Oligomers through Spatially Separated Triplet Pair States. *Nat. Chem.* **2021**, *13* (6), 559–567. https://doi.org/10.1038/s41557-021-00665-7.

(66) Baluschev, S.; Yakutkin, V.; Miteva, T.; Avlasevich, Y.; Chernov, S.; Aleshchenkov, S.; Nelles, G.; Cheprakov, A.; Yasuda, A.; Müllen, K.; Wegner, G. Blue-Green up-Conversion: Noncoherent Excitation by NIR Light. *Angew. Chemie - Int. Ed.* **2007**, *46* (40), 7693–7696. https://doi.org/10.1002/anie.200700414.

(67) Hetzer, C.; Guldi, D. M.; Tykwinski, R. R. Pentacene Dimers as a Critical Tool for the Investigation of Intramolecular Singlet Fission. *Chem. - A Eur. J.* **2018**, *24* (33), 8245–8257. https://doi.org/10.1002/chem.201705355.

(68) Abraham, V.; Mayhall, N. J. Simple Rule to Predict Boundedness of Multiexciton States in Covalently Linked Singlet-Fission Dimers. *J. Phys. Chem. Lett.* **2017**, *8* (22), 5472–5478. https://doi.org/10.1021/acs.jpclett.7b02476.

(69) Mardazad, S.; Xu, Y.; Yang, X.; Grundner, M.; Schollwöck, U.; Ma, H.; Paeckel, S. Quantum Dynamics Simulation of Intramolecular Singlet Fission in Covalently Linked Tetracene Dimer. *J. Chem. Phys.* **2021**, *155* (19). https://doi.org/10.1063/5.0068292.

(70) Zirzlmeier, J.; Lehnherr, D.; Coto, P. B.; Chernick, E. T.; Casillas, R.; Basel, B. S.; Thoss, M.; Tykwinski, R. R.; Guldi, D. M. Singlet Fission in Pentacene Dimers. *Proc. Natl. Acad. Sci. U. S. A.* **2015**, *112* (17), 5325–5330. https://doi.org/10.1073/pnas.1422436112.

(71) Iwanaga, T.; Yamamoto, Y.; Nishioka, K.; Toyota, S. Efficient Synthesis and Electronic Spectra of Unsymmetrical 5,12-Diethynyltetracene Derivatives. *Synth.* **2015**, *47* (24), 3997–4007. https://doi.org/10.1055/s-0035-1560474.

(72) Lehnherr, D.; McDonald, R.; Tykwinski, R. R. Exploring Electronically Polarized Pentacenes. *Org. Lett.* **2008**, *10* (19), 4163–4166. https://doi.org/10.1021/ol801464k.

(73) Kasha, M.; Rawls, H. R.; El-Bayoumi, M. A. The Exciton Model In Molecular Spectroscopy. *Pure Appl. Chem.* **1965**, *11* (3–4), 371–392. https://doi.org/10.1351/pac196511030371.

(74) The Splitting between the $^{1}(T_1T_1)$ and $^{5}(T_1T_1)$ in **MAdTc$_2$** is less than the resolution of theprogram output.

(75) Dral, P. O.; Clark, T. Semiempirical UNO-CAS and UNO-CI: Method and Applications in Nanoelectronics. *J. Phys. Chem. A* **2011**, *115* (41), 11303–11312. https://doi.org/10.1021/jp204939x.

(76) For MPhTc2 in Benzonitrile, the Slow Solvent Rearrangement of (S1S0) in Viscous Benzonitrile and the Fast Formation of the Third Species Hampers Clearly Distinguishing between (S1S0) and (S1S0)Rel. 2.

(77) Sanders, S. N.; Pun, A. B.; Parenti, K. R.; Kumarasamy, E.; Yablon, L. M.; Sfeir, M. Y.; Campos, L. M. Understanding the Bound Triplet-Pair State in Singlet Fission. *Chem* **2019**, *5* (8), 1988–2005. https://doi.org/10.1016/j.chempr.2019.05.012.

(78) Lissi, E. A.; Encinas, M. V.; Lemp, E.; Rubio, M. A. Singlet Oxygen O2(1Δg) Bimolecular Processes. Solvent and Compartmentalization Effects. *Chem. Rev.* **1993**, *93* (2), 699–723. https://doi.org/10.1021/cr00018a004.

(79) Murakami, Y.; Kamada, K. Kinetics of Photon Upconversion by Triplet-Triplet Annihilation: A Comprehensive Tutorial. *Phys. Chem. Chem. Phys.* **2021**, *23* (34), 18268–18282. https://doi.org/10.1039/d1cp02654b.

(80) Haefele, A.; Blumhoff, J.; Khnayzer, R. S.; Castellano, F. N. Getting to the (Square) Root of the Problem: How to Make Noncoherent Pumped Upconversion Linear. *J. Phys. Chem. Lett.* **2012**, *3* (3), 299–303. https://doi.org/10.1021/jz300012u.

(81) Zhu, T.; Huang, L. Exciton Transport in Singlet Fission Materials: A New Hare and Tortoise Story. *J. Phys. Chem. Lett.* **2018**, *9* (22), 6502–6510.

https://doi.org/10.1021/acs.jpclett.8b02181.
(82) Piland, G. B.; Burdett, J. J.; Dillon, R. J.; Bardeen, C. J. Singlet Fission: From Coherences to Kinetics. *J. Phys. Chem. Lett.* **2014**, *5* (13), 2312–2319. https://doi.org/10.1021/jz500676c.
(83) Taffet, E. J.; Beljonne, D.; Scholes, G. D. Overlap-Driven Splitting of Triplet Pairs in Singlet Fission. *J. Am. Chem. Soc.* **2020**, *142* (47), 20040–20047. https://doi.org/10.1021/jacs.0c09276.
(84) Bossanyi, D. G.; Matthiesen, M.; Wang, S.; Smith, J. A.; Kilbride, R. C.; Shipp, J. D.; Chekulaev, D.; Holland, E.; Anthony, J. E.; Zaumseil, J.; Musser, A. J.; Clark, J. Emissive Spin-0 Triplet-Pairs Are a Direct Product of Triplet–Triplet Annihilation in Pentacene Single Crystals and Anthradithiophene Films. *Nat. Chem.* **2021**, *13* (2), 163–171. https://doi.org/10.1038/s41557-020-00593-y.
(85) The Uncertainty Is given by the Standard Deviation of the Slope Fit to the Data Using a Linear Regression.Pdf.
(86) The Value Is Based on Data Points at 300 and 230 K.
(87) As for **mPhTc$_2$** in benzonitrile, (S_1S_0) and $(S_1S_0)_{Rel}$ are Indistinguishable in MeTHF as Well.
(88) Φr-T Is Used to Compare the Trend of Triplet Excited Formation at Different Temperatures. It Should Be Noted That There Is No Absolute Meaning since the Intermediated State (S1S0)(T1T1)CT Is Not a Pure Singlet Excited State. 1. The relative triplet quantum yield of (T_1T_1) ($\Phi_{r\text{-}T}$) is given by $\Phi_{r\text{-}T} = I((T_1T_1))/I((S_1S_0)_{(T1T1)^{CT}})$, where I is the intensity of the ground state bleaching minimum of the respective species.

Table of Contents